UWThPh-2000-06
HEPHY-PUB 729/00
FTUV/00-10
IFIC/00-10
hep-ph/0002115
LC-TH-2000-031

Phenomenology of Stops, Sbottoms, τ-Sneutrinos, and Staus at an e^+e^- Linear Collider

A. Bartl,[1] H. Eberl,[2] S. Kraml,[2] W. Majerotto,[2] W. Porod[3]

[1] *Institut für Theoretische Physik, Universität Wien, A–1090 Vienna, Austria*
[2] *Inst. f. Hochenergiephysik, Österr. Akademie d. Wissenschaften, A–1050 Vienna, Austria*
[3] *Inst. de Física Corpuscular (IFIC), CSIC, E–46071 València, Spain*

Abstract

We discuss production and decays of stops, sbottoms, τ-sneutrinos, and staus in e^+e^- annihilation in the energy range $\sqrt{s} = 0.5 - 1$ TeV. We present numerical predictions within the Minimal Supersymmetric Standard Model for cross sections and decay rates, including one–loop radiative corrections as well as initial state radiation. We also study the importance of beam polarization for the determination of the underlying SUSY parameters. Moreover, we make a comparison of the potential to study squarks and sleptons of the 3rd generation between Tevatron, LHC, and Linear Collider.

1 Introduction

In supersymmetric (SUSY) extensions of the Standard Model (SM) squarks $\tilde{q}_L$, $\tilde{q}_R$, sleptons $\tilde{\ell}_L$, $\tilde{\ell}_R$, and sneutrinos $\tilde{\nu}_\ell$ are introduced as the scalar partners of the quarks $q_{L,R}$, leptons $\ell_{L,R}$, and neutrinos ν_ℓ [1]. For each sfermion of definite flavour the states $\tilde{f}_L$ and $\tilde{f}_R$ are interaction states which are mixed by Yukawa terms. The mass eigenstates are denoted by $\tilde{f}_1$ and $\tilde{f}_2$ (with the convention $m_{\tilde{f}_1} < m_{\tilde{f}_2}$). Strong $\tilde{f}_L - \tilde{f}_R$ mixing is expected for the third generation sfermions, because in this case the Yukawa couplings can be large. In particular, in the sector of the scalar top quarks these mixing effects will be large due to the large top quark mass. The lighter mass eigenstate $\tilde{t}_1$ will presumably be the lightest squark state [2, 3]. If the SUSY parameter $\tan\beta$ is large, $\tan\beta \gtrsim 10$, then also $\tilde{b}_L - \tilde{b}_R$ and $\tilde{\tau}_L - \tilde{\tau}_R$ mixing has to be taken into account and will lead to observable effects [4, 5]. The experimental search for the third generation sfermions is an important issue at all present and future colliders. It will be particularly interesting at an e^+e^- Linear Collider with center of mass energy $\sqrt{s} = 0.5 - 1.5$ TeV, where these states are expected to be pair produced. Moreover, at an e^+e^- Linear Collider with this energy and an integrated luminosity of about 500 fb^{-1} it will be possible to measure masses, cross sections and decay branching ratios with high precision [6]. This will allow us to obtain information on the fundamental soft SUSY breaking parameters. Therefore, it is necessary to investigate how this information can be extracted from the experimental data, and how precisely these parameters can be determined. In this way it will be possible to test our theoretical ideas about the underlying SUSY breaking mechanism.

Contribution to the Proceedings of the "2nd Joint ECFA/DESY Study on Physics and Detectors for a Linear Electron–Positron Collider".

Phenomenological studies on SUSY particle searches at the LHC have shown that the detection of the scalar top quark may be very difficult due to the overwhelming background from $t\bar{t}$ production [7, 8, 9]. This is in particular true for $m_{\tilde{t}_1} \lesssim 250$ GeV [7]. In principle, such a light stop could be discovered at the Tevatron. The actual mass reach, however, strongly depends on the luminosity, decay modes, and the available phase–space [10, 11]. Thus an e^+e^- Linear Collider with $\sqrt{s} \sim 500$ GeV could even be a discovery machine for $\tilde{t}_1$.

In this contribution we summarize the phenomenology of $\tilde{t}$, $\tilde{b}$, $\tilde{\tau}$, and $\tilde{\nu}_\tau$ in e^+e^- annihilation at energies between $\sqrt{s} = 500$ GeV and 1 TeV. We give numerical results for the production cross sections taking into account polarization of both the e^- and e^+ beams. In particular, we show that by using polarized beams it will be possible to determine the fundamental SUSY parameters with higher precision than without polarization. Moreover, we discuss the decays of these particles. The production cross sections as well as the decay rates of the sfermions show a distinct dependence on the $\tilde{f}_L$–$\tilde{f}_R$ mixing angles. Squarks (sleptons) can decay into quarks (leptons) plus neutralinos or charginos. Squarks may also decay into gluinos. In addition, if the splitting between the different sfermion mass eigenstates is large enough, transitions between these states by emmission of weak vector bosons or Higgs bosons are possible. These decay modes can be important for the higher mass eigenstates, and lead to complicated cascade decays. In the case of the lighter stop, however, all these tree–level two–body decays may be kinematically forbidden. Then the $\tilde{t}_1$ has more complicated higher–order decays [12, 13, 14].

The framework of our calculation is the Minimal Supersymmetric Standard Model (MSSM) [1] which contains the Standard Model (SM) particles plus the sleptons $\tilde{\ell}^\pm$, sneutrinos $\tilde{\nu}_\ell$, squarks $\tilde{q}$, gluinos $\tilde{g}$, two pairs of charginos $\tilde{\chi}^\pm_i$, $i = 1, 2$, four neutralinos, $\tilde{\chi}^0_i$, $i = 1, \ldots, 4$, and five Higgs bosons, h^0, H^0, A^0, $H^\pm$ [15].

In Section 2 we shortly review the basic features of left–right mixing of squarks and sleptons of the 3rd generation, and present formulae and numerical results for the production cross sections with polarized e^- and e^+ beams. In Section 3 we discuss the decays of these particles and present numerical results for their branching ratios. In Section 4 we give an estimate of the errors to be expected for the fundamental soft SUSY–breaking parameters of the stop mixing matrix. In Section 5 we compare the situation concerning stop, sbottom, and stau searches at LHC and Tevatron with that at an e^+e^- Linear Collider. Section 6 contains a short summary.

2 Production Cross Sections

Left–right mixing of the sfermions is described by the symmetric 2×2 mass matrices which in the $(\tilde{f}_L, \tilde{f}_R)$ basis $(f = t, b, \tau)$ read [2, 15]

$$\mathcal{M}^2_{\tilde{f}} = \begin{pmatrix} M^2_{\tilde{f}_L} & a_f m_f \\ a_f m_f & M^2_{\tilde{f}_R} \end{pmatrix} . \tag{1}$$

The diagonal elements of the sfermion mass matrices are

$$M^2_{\tilde{f}_L} = M^2_{\tilde{F}} + m^2_Z \cos 2\beta (T^3_f - e_f \sin^2 \Theta_W) + m^2_f \,, \tag{2}$$

$$M^2_{\tilde{f}_R} = M^2_{\tilde{F}'} + e_f m^2_Z \cos 2\beta \sin^2 \theta_W + m^2_f \tag{3}$$

where m_f, e_f and T^3_f are the mass, charge and third component of weak isospin of the fermion f, and θ_W is the Weinberg angle. Moreover, $M_{\tilde{F}} = M_{\tilde{Q}}$ for $\tilde{f}_L = \tilde{t}_L, \tilde{b}_L$, $M_{\tilde{F}} = M_{\tilde{L}}$ for $\tilde{f}_L = \tilde{\tau}_L$, and $M_{\tilde{F}'} = M_{\tilde{U}}, M_{\tilde{D}}, M_{\tilde{E}}$ for $\tilde{f}_R = \tilde{t}_R, \tilde{b}_R, \tilde{\tau}_R$, respectively. $M_{\tilde{Q}}$, $M_{\tilde{U}}$, $M_{\tilde{D}}$, $M_{\tilde{L}}$, and $M_{\tilde{E}}$ are soft SUSY–breaking mass parameters of the third generation sfermion system. The off–diagonal elements of the sfermion mass matrices are

$$m_t a_t = m_t (A_t - \mu \cot \beta) \,, \tag{4}$$

$$m_b a_b = m_b(A_b - \mu\tan\beta)\,, \tag{5}$$
$$m_\tau a_\tau = m_\tau(A_\tau - \mu\tan\beta) \tag{6}$$

for stop, sbottom, and stau, respectively. A_t, A_b, A_τ are soft SUSY–breaking trilinear scalar coupling parameters. Evidently, in the stop sector there can be strong $\tilde{t}_L$-$\tilde{t}_R$ mixing due to the large top quark mass. In the case of sbottoms and staus the $\tilde{f}_L - \tilde{f}_R$ mixing effects are also non-negligible if $\tan\beta \gtrsim 10$. We assume that all parameters are real. Then the mass matrices can be diagonalized by 2×2 orthogonal matrices. The mass eigenvalues for the sfermions $\tilde{f} = \tilde{t}, \tilde{b}, \tilde{\tau}$ are

$$m^2_{\tilde{f}_{1,2}} = \frac{1}{2}(M^2_{\tilde{f}_L} + M^2_{\tilde{f}_R} \mp \sqrt{(M^2_{\tilde{f}_L} - M^2_{\tilde{f}_R})^2 + 4m_f^2 a_f^2}\,)\,, \tag{7}$$

and the mass eigenstates are

$$\tilde{f}_1 = \tilde{f}_L\cos\theta_{\tilde{f}} + \tilde{f}_R\sin\theta_{\tilde{f}}\,, \tag{8}$$
$$\tilde{f}_2 = \tilde{f}_R\cos\theta_{\tilde{f}} - \tilde{f}_L\sin\theta_{\tilde{f}}\,, \tag{9}$$

where $\tilde{t}_1$, $\tilde{b}_1$, $\tilde{\tau}_1$ denote the lighter eigenstates. The sfermion mixing angle is given by

$$\cos\theta_{\tilde{f}} = \frac{-a_f m_f}{\sqrt{(M^2_{\tilde{f}_L} - m^2_{\tilde{f}_1})^2 + a_f^2 m_f^2}}\,, \qquad \sin\theta_{\tilde{f}} = \frac{M^2_{\tilde{f}_L} - m^2_{\tilde{f}_1}}{\sqrt{(M^2_{\tilde{f}_L} - m^2_{\tilde{f}_1})^2 + a_f^2 m_f^2}}\,. \tag{10}$$

The $\tilde{\nu}_\tau$ appears only in the left–state. Its mass is

$$m^2_{\tilde{\nu}_\tau} = M^2_{\tilde{L}} + \frac{1}{2}m_Z^2\cos 2\beta\,. \tag{11}$$

The reaction $e^+e^- \to \tilde{f}_i\bar{\tilde{f}}_j$ proceeds via γ and Z exchange in the s–channel. For polarized e^- and e^+ beams the cross section of this reaction at tree level has the form [16]

$$\begin{aligned}\sigma^0 = \frac{\pi\alpha^2\kappa_{ij}^3}{s^4}\Bigg\{ & e_f^2\delta_{ij}(1-\mathcal{P}_-\mathcal{P}_+) - \frac{e_f c_{ij}\delta_{ij}}{2s_W^2c_W^2}\left[v_e(1-\mathcal{P}_-\mathcal{P}_+) - a_e(\mathcal{P}_- - \mathcal{P}_+)\right] D_{\gamma Z} \\ & + \frac{c_{ij}^2}{16s_W^4c_W^4}\left[(v_e^2+a_e^2)(1-\mathcal{P}_-\mathcal{P}_+) - 2v_ea_e(\mathcal{P}_- - \mathcal{P}_+)\right] D_{ZZ}\Bigg\}\,, \end{aligned} \tag{12}$$

where $\mathcal{P}_-$ and $\mathcal{P}_+$ denote the degree of polarization of the e^- and e^+ beams, with the convention $\mathcal{P}_\pm = -1, 0, +1$ for left–polarized, unpolarized, right–polarized $e^\pm$ beams, respectively. (E.g., $\mathcal{P}_- = -0.9$ means that 90% of the electrons are left–polarized and the rest is unpolarized.) $v_e = 4s_W^2 - 1$, $a_e = -1$ are the vector and axial–vector couplings of the electron to the Z, $s_W^2 \equiv \sin^2\theta_W$, $c_W^2 \equiv \cos^2\theta_W$, and c_{ij} is the $Z\tilde{f}_i\tilde{f}_j$ coupling (up to a factor $1/\cos\theta_W$)

$$c_{ij} = \begin{pmatrix} T_f^3\cos^2\theta_{\tilde{f}} - e_f s_W^2 & -\frac{1}{2}T_f^3\sin 2\theta_{\tilde{f}} \\ -\frac{1}{2}T_f^3\sin 2\theta_{\tilde{f}} & T_f^3\sin^2\theta_{\tilde{f}} - e_f s_W^2 \end{pmatrix}\,. \tag{13}$$

Furthermore, in Eq. (12) $\sqrt{s}$ is the center–of–mass energy, $\kappa_{ij} = [(s - m^2_{\tilde{f}_i} - m^2_{\tilde{f}_j})^2 - 4m^2_{\tilde{f}_i}m^2_{\tilde{f}_j}]^{1/2}$, and

$$D_{ZZ} = \frac{s^2}{(s-m_Z^2)^2 + \Gamma_Z^2 m_Z^2}\,, \qquad D_{\gamma Z} = \frac{s(s-m_Z^2)}{(s-m_Z^2)^2 + \Gamma_Z^2 m_Z^2}\,. \tag{14}$$

The cross section in Eq. (12) depends on the sfermion mixing parameters, because the $Z\tilde{f}_i\bar{\tilde{f}}_j$ couplings Eq. (13)) depend on the mixing angles. For example, the couplings $Z\tilde{t}_1\bar{\tilde{t}}_1$, $Z\tilde{b}_1\bar{\tilde{b}}_1$, and $Z\tilde{\tau}_1\bar{\tilde{\tau}}_1$ vanish at

$\theta_{\tilde{t}} = 0.98$, $\theta_{\tilde{b}} = 1.17$, and $\theta_{\tilde{\tau}} = 0.82$, respectively. There is a destructive interference between the γ and Z–exchange contributions that leads to characteristic minima of the cross sections at specific values of the mixing angles $\theta_{\tilde{f}}$, which according to Eq. (12) depend on $\sqrt{s}$ and on the beam polarizations $\mathcal{P}_-$ and $\mathcal{P}_+$ [17].

In Figs. 1 a, b we show the $\sqrt{s}$ dependence of the stop and sbottom pair production cross sections for $m_{\tilde{t}_1} = 220$ GeV, $m_{\tilde{t}_2} = 450$ GeV, $\cos\theta_{\tilde{t}} = -0.66$, $m_{\tilde{b}_1} = 284$ GeV, $m_{\tilde{b}_2} = 345$ GeV, $\cos\theta_{\tilde{b}} = 0.84$, and $m_{\tilde{g}} = 555$ GeV. Here we have included supersymmetric QCD (i.e. gluon and gluino) corrections [19, 20] and initial state radiation (ISR) [21]. [1] The latter typically changes the cross section by $\sim 15\%$. The relative importance of the gluon and gluino corrections can be seen in Figs. 1 c, d where we plot $\Delta\sigma/\sigma^0$ for $\tilde{t}_1\bar{\tilde{t}}_2$ and $\tilde{b}_1\bar{\tilde{b}}_1$ production for the parameters of Fig. 1 a, b. In addition we also show the leading electroweak corrections in order of Yukawa couplings squared [22] for $M = 200$ GeV, $\mu = 800$ GeV, $m_A = 300$ GeV, and $\tan\beta = 4$. Let us discuss these corrections in more detail:

The standard QCD correction [19] (due to virtual gluon exchange and real gluon emission) is proportional to the tree–level cross section: $\sigma = \sigma^0\,(1+\frac{4\alpha_s}{3\pi}\Delta)$ with Δ depending on the velocity of the outgoing squarks. In the high energy limit $\beta = 1 - 4m^2_{\tilde{q}_i}/s \to 1$ we have $\Delta = 3$, i.e. the gluonic correction amounts to 10–15% of σ^0. Notice that this is four times the corresponding correction for quark production. At/near the threshold, colour–Coulomb effects have to be taken into account [23]. These lead to $\Delta \simeq \pi^2/(2\beta) - 2$ near the threshold. Very close to threshold the perturbation expansion becomes unreliable, and the non–perturbative contribution leads to a constant cross section for $\beta = 0$. Moreover, bound state formation is felt in this region. A recent study [24] concluded that these bound states cannot be detected at an e^+e^- Linear Collider. Still they may affect the precision of a mass determination of squarks by threshold scans. (Further investigations are necessary for quantitative results.) On the other hand, measuring the β^3 rise of the cross section, as well as the $\sin^2\vartheta$ dependence of the differential cross section (ϑ being the scattering angle), will be useful for confirming the spin-0 character of squarks and sleptons.

The gluon correction has clearly the largest effect. However, for precision measurements also gluino exchange [20] has to be taken into account. In contrast to the former, which is always positive, the gluino correction can be of either sign. Moreover, it does not factorize with the tree level but leads to an additional dependence on the squark mixing angle. The same holds for Yukawa coupling corrections [22]. It turned out that these corrections can be quite large, up to $\pm 10\%$ for squark production, depending on the properties of the charginos, neutralinos, Higgs bosons, and squarks in the loops. In the remaining part of this section we will, however, not include Yukawa coupling corrections because they depend on the whole MSSM spectrum.

Figure 2 shows the cross sections for $\tilde{\tau}$ and $\tilde{\nu}_\tau$ production for $m_{\tilde{\tau}_1} = 156$ GeV, $m_{\tilde{\tau}_2} = 180$ GeV, $\cos\theta_{\tilde{\tau}} = 0.77$, and $m_{\tilde{\nu}_\tau} = 148$ GeV. As can be seen, these cross sections can be comparable in size to $\tilde{t}_1\bar{\tilde{t}}_1$ production. In Fig. 2 we have included only ISR. Yukawa coupling corrections are below the percent level for this choice of parameters and e.g., $M = 200$ GeV, $\mu = 800$ GeV, $m_A = 300$ GeV, $\tan\beta = 4$. They can, however, go up to $\sim 5\%$ in certain parameter regions, especially for large $\tan\beta$, see [22].

Let us now turn to the dependence on the mixing angles and beam polarizations. In Fig. 3 we show $\sigma(e^+e^- \to \tilde{t}_i\bar{\tilde{t}}_i)$ as a function of $\cos\theta_{\tilde{t}}$ for $m_{\tilde{t}_1} = 200$ GeV, $m_{\tilde{t}_2} = 420$ GeV, $m_{\tilde{g}} = 555$ GeV, $\sqrt{s} = 500$ GeV in (a) and $\sqrt{s} = 1$ TeV in (b). The full lines are for unpolarized beams, the dashed lines are for a 90% polarized e^- beam, and the dotted ones for 90% polarized e^- and 60% polarized e^+ beams. As one can see, beam polarization strengthens the $\cos\theta_{\tilde{t}}$ dependence and can thus be essential for determining the mixing angle. Moreover, it can be used to enhance the signal and/or reduce the background.

In Figs. 4 a, b we show the contour lines of the cross section $\sigma(e^+e^- \to \tilde{t}_1\bar{\tilde{t}}_1)$ as a function of the e^- and e^+ beam polarizations $\mathcal{P}_-$ and $\mathcal{P}_+$ at $\sqrt{s} = 500$ GeV for two values of $\cos\theta_{\tilde{t}}$: $\cos\theta_{\tilde{t}} = 0.4$ in (a) and $\cos\theta_{\tilde{t}} = 0.66$ in (b). The white windows show the range of polarization of the TESLA design [25]. As

[1] The Fortran program [18] is available on the Web.

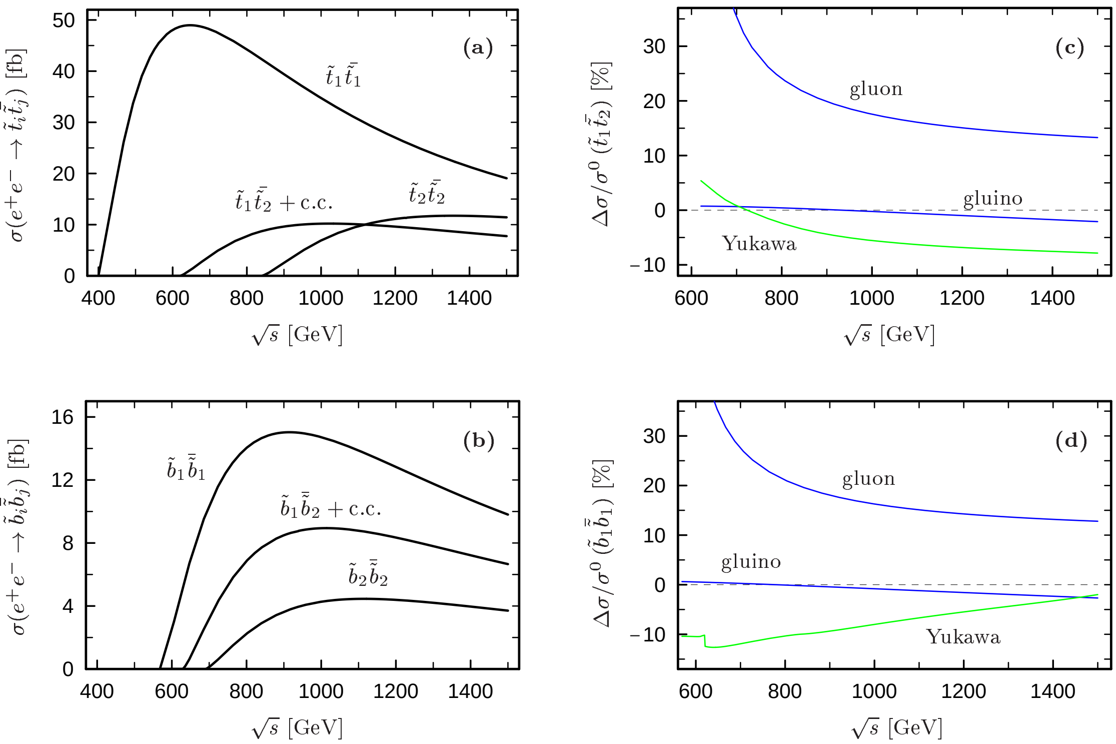

Figure 1: $(\mathbf{a}, \mathbf{b})$ Total cross sections for $e^+e^- \to \tilde{t}_i\bar{\tilde{t}}_j$, $\tilde{b}_i\bar{\tilde{b}}_j$ as a function of $\sqrt{s}$ for $m_{\tilde{t}_1} = 200$ GeV, $m_{\tilde{t}_2} = 420$ GeV, $\cos\theta_{\tilde{t}} = -0.66$, $m_{\tilde{b}_1} = 284$ GeV, $m_{\tilde{b}_2} = 345$ GeV, $\cos\theta_{\tilde{b}} = 0.84$, and $m_{\tilde{g}} = 555$ GeV; included are SUSY–QCD and ISR corrections. $(\mathbf{c}, \mathbf{d})$ gluon, gluino, and Yukawa coupling corrections relative to the tree level cross section of $\tilde{t}_1\bar{\tilde{t}}_2$ and $\tilde{b}_1\bar{\tilde{b}}_1$ production for $M = 200$ GeV, $\mu = 800$ GeV, $\tan\beta = 4$, $m_A = 300$ GeV, and the other parameters as in (a, b).

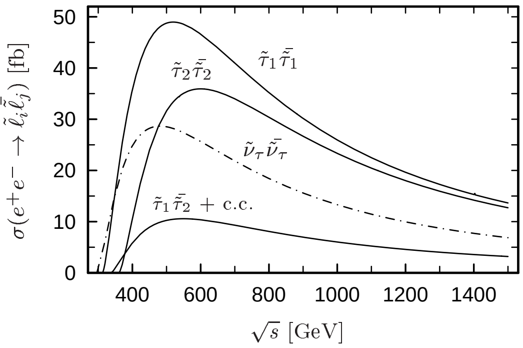

Figure 2: Total cross sections of stau and sneutrino pair production as a function of $\sqrt{s}$ for $m_{\tilde{\tau}_1} = 156$ GeV, $m_{\tilde{\tau}_2} = 180$ GeV, $\cos\theta_{\tilde{\tau}} = 0.77$, and $m_{\tilde{\nu}_\tau} = 148$ GeV.

one can see, one can significantly increase the cross section by using the maximally possible e^- *and* e^+ polarization. Here note that the (additional) positron polarization leads to an effective polarization [26] of

$$\mathcal{P}_{\rm eff} = \frac{\mathcal{P}_- - \mathcal{P}_+}{1 - \mathcal{P}_-\mathcal{P}_+} \, . \tag{15}$$

In experiments with polarized beams one can also measure the left–right asymmetry

$$A_{LR} \equiv \frac{\sigma_L - \sigma_R}{\sigma_L + \sigma_R} \tag{16}$$

where $\sigma_L := \sigma\,(-|\mathcal{P}_-|, |\mathcal{P}_+|)$ and $\sigma_R := \sigma\,(|\mathcal{P}_-|, -|\mathcal{P}_+|)$. This observable is sensitive to the amount of mixing of the produced sfermions while kinematical effects only enter at loop level. In Fig. 5 we show A_{LR} for $e^+e^- \to \tilde t_i \bar{\tilde t}_i$ $(i = 1, 2)$ as a function of $\cos\theta_{\tilde t}$ for 90% polarized electrons and unpolarized as well as 60% polarized positrons; $\sqrt{s} = 1$ TeV and the other parameters are as in Fig. 3.

Last but not least we note that the reaction $e^+e^- \to \tilde t_1 \tilde t_2$ (with $\tilde t_1 \tilde t_2 \equiv \tilde t_1 \bar{\tilde t}_2 + \mathrm{c.c.}$) can be useful to measure $m_{\tilde t_2}$ below the $\tilde t_2 \bar{\tilde t}_2$ threshold. As this reaction proceeds only via Z exchange the cross section shows a clear $\sin 2\theta_{\tilde t}$ dependence. $\sigma(e^+e^- \to \tilde t_1 \tilde t_2)$ can be enhanced by using left–polarized electrons. The additional use of right–polarized positrons further enhances the cross section. To give an example, for $m_{\tilde t_1} = 200$ GeV, $m_{\tilde t_2} = 420$ GeV, $\cos\theta_{\tilde t} = 0.7$, and $\sqrt{s} = 800$ GeV we obtain $\sigma(\tilde t_1 \tilde t_2) = 7.9$ fb, 9.1 fb, and 14.1 fb for $(\mathcal{P}_-, \mathcal{P}_+) = (0, 0)$, $(-0.9, 0)$, and $(-0.9, 0.6)$, respectively. The left–right asymmetry, however, hardly varies with $\cos\theta_{\tilde t}$: $A_{LR}(\tilde t_1 \tilde t_2) \simeq 0.14$ (0.15) for $|\mathcal{P}_-| = 0.9$ and $|\mathcal{P}_+| = 0$ (0.6), $0 < |\cos\theta_{\tilde t}| < 1$, and the other parameters as above.

We next discuss sbottom production using the scenario of Fig. 1 b, i.e. $m_{\tilde b_1} = 284$ GeV and $m_{\tilde b_2} = 345$ GeV. In this case, all three combinations $\tilde b_1 \bar{\tilde b}_1$, $\tilde b_1 \tilde b_2$ $(\equiv \tilde b_1 \bar{\tilde b}_2 + \tilde b_2 \bar{\tilde b}_1)$, and $\tilde b_2 \bar{\tilde b}_2$ can be produced at $\sqrt{s} =$ 800 GeV. The $\cos\theta_{\tilde b}$ dependence of the corresponding cross sections are shown in Fig. 6 for unpolarized, 90% left–, and 90% right–polarized electrons ($\mathcal{P}_+ = 0$). As can be seen, beam polarization can be a useful tool to disentangle $\tilde b_1$ and $\tilde b_2$.

The left–right asymmetry A_{LR}, Eq. (16), of $\tilde b_1 \bar{\tilde b}_1$ and $\tilde b_2 \bar{\tilde b}_2$ production is shown in Fig. 7 as a function of $\cos\theta_{\tilde b}$ for 90% polarized e^- and unpolarized as well as 60% polarized e^+ beams. As in the case of stop production, $A_{LR}(\tilde b_i \bar{\tilde b}_i)$ is very sensitive to the left–right mixing.

The explicit dependence on the e^- and e^+ beam polarizations can be seen in Fig. 8 where we plot the contourlines of $\sigma(e^+e^- \to \tilde b_1 \bar{\tilde b}_1)$ and $\sigma(e^+e^- \to \tilde b_2 \bar{\tilde b}_2)$ as functions of $\mathcal{P}_-$ and $\mathcal{P}_+$ for the parameters used above and $\cos\theta_{\tilde b} = 0.84$. Again, the white windows indicate the range of the TESLA design. Also in this case we observe that one can considerably increase the cross section by rising the effective polarization.

The renormalization group equations [27] for the slepton parameters are different from those for the squarks. Moreover, owing to Yukawa coupling effects, the parameters of the 3rd generation evolve differently compared to those of the 1st and 2nd generation. Therefore, measuring the properties of the squarks as well as the sleptons quite precisely will be necessary to test the boundary conditions at the GUT scale and the SUSY breaking mechanism.

In the following plots on $\tilde\tau$ and $\tilde\nu_\tau$ pair production we fix $m_{\tilde\tau_1} = 156$ GeV, $m_{\tilde\tau_2} = 180$ GeV, and $m_{\tilde\nu} = 148$ GeV as in Fig. 2. In the calculation of the cross sections we include ISR corrections which turn out to be of the order of 10–15%. Figure 9 shows the $\cos\theta_{\tilde\tau}$ dependence of $\tilde\tau_i \bar{\tilde\tau}_j$ production at $\sqrt{s} = 500$ GeV for unpolarized as well as for polarized e^- beams ($\mathcal{P}_+ = 0$). The usefulness of beam polarization to (i) increase the $\cos\theta_{\tilde\tau}$ dependence and (ii) enhance/reduce $\tilde\tau_1 \bar{\tilde\tau}_1$ relative to $\tilde\tau_2 \bar{\tilde\tau}_2$ production is obvious. The left–right asymmetry of $\tilde\tau_i \bar{\tilde\tau}_i$ production for the parameters of Fig. 9 is shown in Fig. 10. Here note that, in contrast to $\tilde t$ and $\tilde b$ production, $A_{LR}(\tilde\tau_i \bar{\tilde\tau}_i)$ is almost zero for maximally mixed staus.

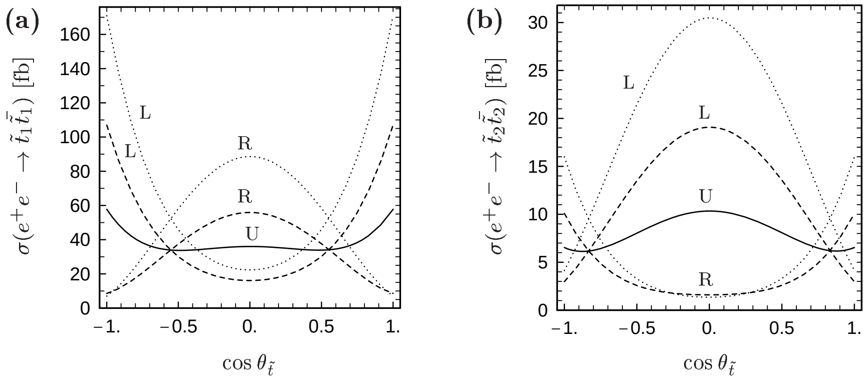

Figure 3: $\cos\theta_{\tilde{t}}$ dependence of stop pair production cross sections for $m_{\tilde{t}_1} = 200$ GeV, $m_{\tilde{t}_2} = 420$ GeV, $m_{\tilde{g}} = 555$ GeV; $\sqrt{s} = 500$ GeV in (a) and $\sqrt{s} = 1$ TeV in (b) ; the label "L" ("R") denotes $\mathcal{P}_- = -0.9$ (0.9) with the dashed lines for $\mathcal{P}_+ = 0$, and the dotted lines for $|\mathcal{P}_+| = 0.6$ [sign$(\mathcal{P}_+) = -$sign$(\mathcal{P}_-)$]; the full lines labeled "U" are for unpolarized beams ($\mathcal{P}_- = \mathcal{P}_+ = 0$).

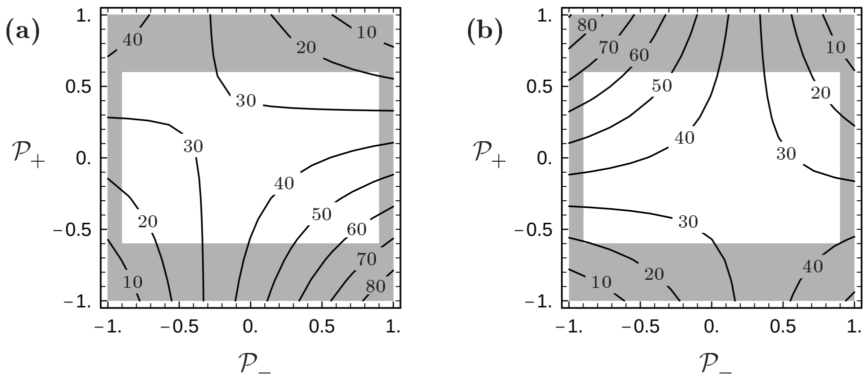

Figure 4: Dependence of $\sigma(e^+e^- \to \tilde{t}_1\bar{\tilde{t}}_1)$ on degree of electron and positron polarization for $\sqrt{s} = 500$ GeV, $m_{\tilde{t}_1} = 200$ GeV, $m_{\tilde{t}_2} = 420$ GeV, and $m_{\tilde{g}} = 555$ GeV; $\cos\theta_{\tilde{t}} = 0.4$ in (a) and $\cos\theta_{\tilde{t}} = 0.66$ in (b).

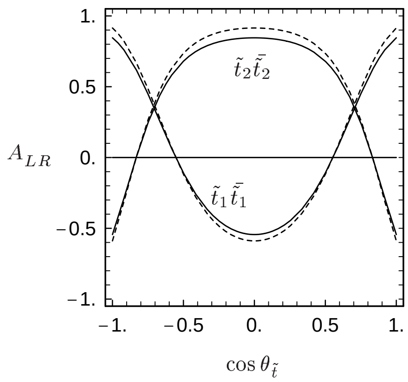

Figure 5: $A_{LR}(e^+e^- \to \tilde{t}_i\bar{\tilde{t}}_i)$ as function of $\cos\theta_{\tilde{t}}$ for $\sqrt{s} = 1$ TeV, $m_{\tilde{t}_1} = 200$ GeV, $m_{\tilde{t}_2} = 420$ GeV, and $m_{\tilde{g}} = 555$ GeV; the solid lines are for 90% polarized electrons and unpolarized positrons, the dashed lines are for 90% polarized electrons and 60% polarized positrons.

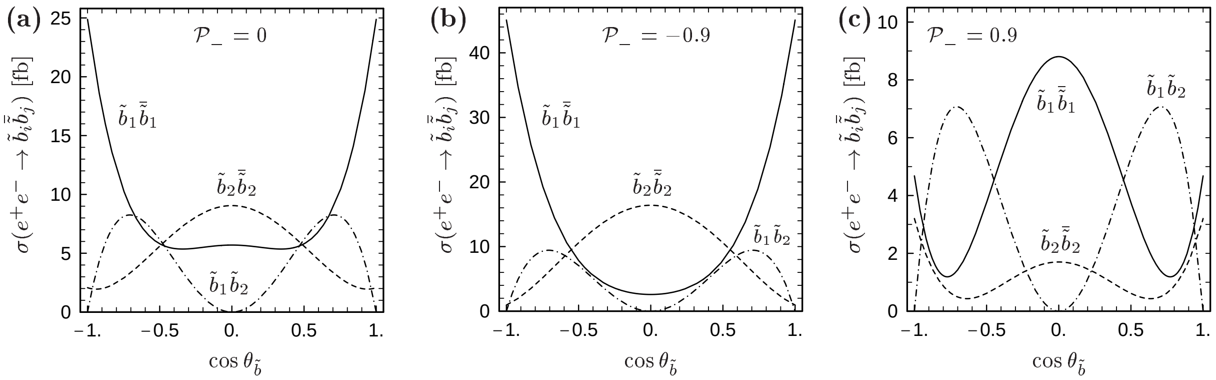

Figure 6: $\cos\theta_{\tilde{b}}$ dependence of sbottom pair production cross sections for $m_{\tilde{b}_1} = 284$ GeV, $m_{\tilde{b}_2} = 345$ GeV, $m_{\tilde{g}} = 555$ GeV, $\sqrt{s} = 800$ GeV and various e^- beam polarizations ($\mathcal{P}_+ = 0$).

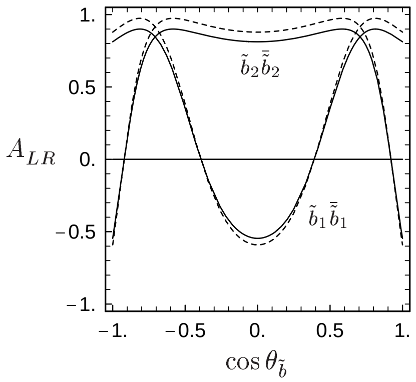

Figure 7: A_{LR} of sbottom pair production as function of $\cos\theta_{\tilde{b}}$ for 90% electron polarization; the full lines are for unpolarized and the dashed lines for 60% polarized positrons; $\sqrt{s} = 800$ GeV, $m_{\tilde{b}_1} = 284$ GeV, $m_{\tilde{b}_2} = 345$ GeV, and $m_{\tilde{g}} = 555$ GeV.

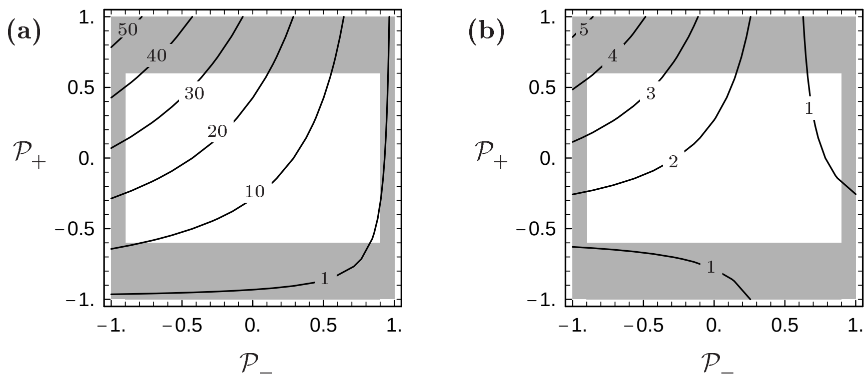

Figure 8: Dependence of (a) $\sigma(e^+e^- \to \tilde{b}_1\bar{\tilde{b}}_1)$ and (b) $\sigma(e^+e^- \to \tilde{b}_2\bar{\tilde{b}}_2)$ (in fb) on the degree of electron and positron polarization for $\sqrt{s} = 800$ GeV, $m_{\tilde{b}_1} = 284$ GeV, $m_{\tilde{b}_2} = 345$ GeV, $\cos\theta_{\tilde{b}} = 0.84$, and $m_{\tilde{g}} = 555$ GeV.

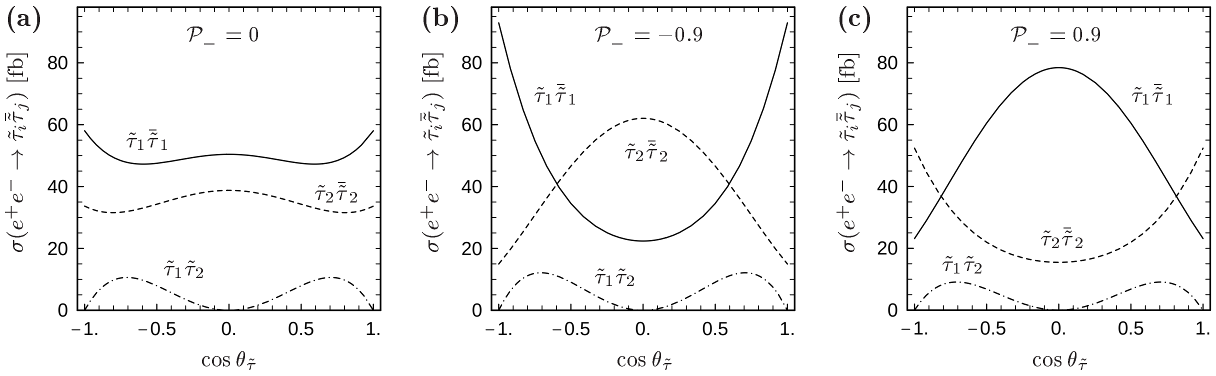

Figure 9: $\cos\theta_{\tilde{\tau}}$ dependence of stau pair production cross sections for $m_{\tilde{\tau}_1} = 156$ GeV, $m_{\tilde{\tau}_2} = 180$ GeV, $\sqrt{s} = 500$ GeV and various e^- beam polarizations ($\mathcal{P}_+ = 0$).

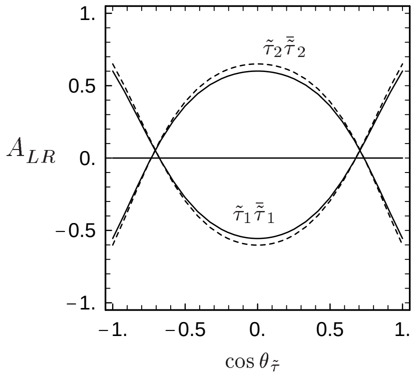

Figure 10: A_{LR} of stau pair production as function of $\cos\theta_{\tilde{\tau}}$ for 90% electron polarization; the full lines are for unpolarized and the dashed lines for 60% polarized positrons; $\sqrt{s} = 500$ GeV, $m_{\tilde{\tau}_1} = 156$ GeV, $m_{\tilde{\tau}_2} = 180$ GeV, and $\cos\theta_{\tilde{\tau}} = 0.77$.

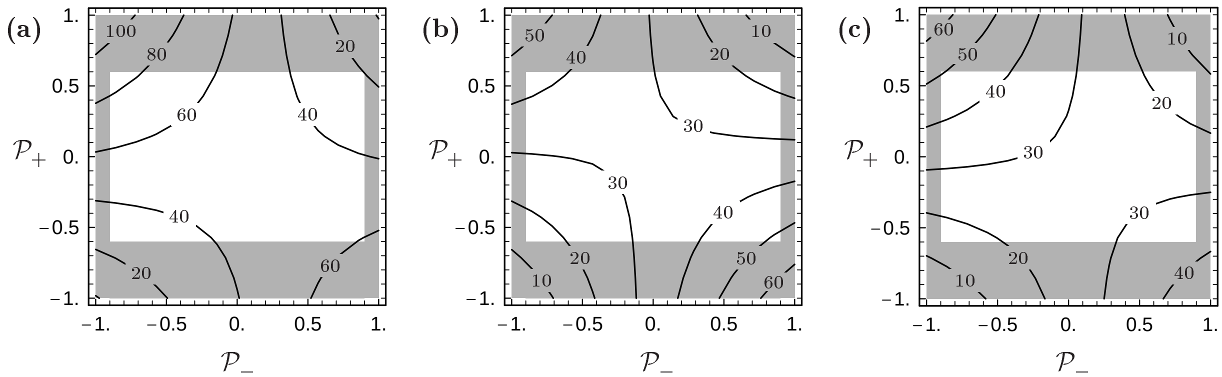

Figure 11: Dependence of (a) $\sigma(e^+e^- \to \tilde{\tau}_1\bar{\tilde{\tau}}_1)$, (b) $\sigma(e^+e^- \to \tilde{\tau}_2\bar{\tilde{\tau}}_2)$, and (c) $\sigma(e^+e^- \to \tilde{\nu}_\tau\bar{\tilde{\nu}}_\tau)$ (in fb) on the degree of electron and positron polarization for $\sqrt{s} = 500$ GeV, $m_{\tilde{\tau}_1} = 156$ GeV, $m_{\tilde{\tau}_2} = 180$ GeV, $\cos\theta_{\tilde{\tau}} = 0.77$, and $m_{\tilde{\nu}_\tau} = 148$ GeV.

Finally, the dependence of $\sigma(e^+e^- \to \tilde{\tau}_i\bar{\tilde{\tau}}_i)$, for $\cos\theta_{\tilde{\tau}} = 0.77$, and $\sigma(e^+e^- \to \tilde{\nu}_\tau\bar{\tilde{\nu}}_\tau)$ on both the electron and positron polarizations is shown in Fig. 11. Notice that one could again substantially increase the cross sections by going beyond 60% e^+ polarization.

3 Decays

Owing to the influence of the Yukawa terms and the left–right mixing, the decay patterns of stops, sbottoms, τ-sneutrinos, and staus are in general more complicated than those of the sfermions of the first two generations. As for the sfermions of the first and second generation, there are the decays into neutralinos or charginos ($i,j = 1,2;\ k = 1,...4$):

$$\tilde{t}_i \to t\,\tilde{\chi}^0_k\,,\ b\,\tilde{\chi}^+_j\,, \qquad \tilde{b}_i \to b\,\tilde{\chi}^0_k\,,\ t\,\tilde{\chi}^-_j\,, \tag{17}$$

$$\tilde{\tau}_i \to \tau\,\tilde{\chi}^0_k\,,\ \nu_\tau\,\tilde{\chi}^-_j\,, \qquad \tilde{\nu}_\tau \to \nu_\tau\,\tilde{\chi}^0_k\,,\ \tau\,\tilde{\chi}^+_j\,. \tag{18}$$

Stops and sbottoms may also decay into gluinos,

$$\tilde{t}_i \to t\,\tilde{g}\,, \qquad \tilde{b}_i \to b\,\tilde{g} \tag{19}$$

and if these decays are kinematically allowed, they are important. If the mass differences $|m_{\tilde{t}_i} - m_{\tilde{b}_j}|$ and/or $|m_{\tilde{\tau}_i} - m_{\tilde{\nu}_\tau}|$ are large enough the transitions

$$\tilde{t}_i \to \tilde{b}_j + W^+\,(H^+) \quad \text{or} \quad \tilde{b}_i \to \tilde{t}_j + W^-\,(H^-) \tag{20}$$

as well as

$$\tilde{\tau}_i \to \tilde{\nu}_\tau + W^-\,(H^-) \quad \text{or} \quad \tilde{\nu}_\tau \to \tilde{\tau}_i + W^+\,(H^+) \tag{21}$$

can occur. Moreover, in case of strong $\tilde{f}_L - \tilde{f}_R$ mixing the splitting between the two mass eigenstates may be so large that heavier sfermion can decay into the lighter one:

$$\tilde{t}_2 \to \tilde{t}_1 + Z^0\,(h^0,H^0,A^0)\,, \quad \tilde{b}_2 \to \tilde{b}_1 + Z^0\,(h^0,H^0,A^0)\,, \quad \tilde{\tau}_2 \to \tilde{\tau}_1 + Z^0\,(h^0,H^0,A^0)\,. \tag{22}$$

The SUSY–QCD corrections to the squark decays of Eqs. (17) to (22) have been calculated in [28]. The Yukawa coupling corrections to the decay $\tilde{b}_i \to t\tilde{\chi}^-_j$ have been discussed in [29]. All these corrections will be important for precision measurements.

The decays of the lighter stop can be still more complicated: If $m_{\tilde{t}_1} < m_{\tilde{\chi}^0_1} + m_t$ and $m_{\tilde{t}_1} < m_{\tilde{\chi}^+_1} + m_b$ the three–body decays [13]

$$\tilde{t}_1 \to W^+ b\,\tilde{\chi}^0_1, \quad H^+ b\,\tilde{\chi}^0_1, \quad b\,\tilde{l}^+_i\,\nu_l, \quad b\,\tilde{\nu}_l\,l^+ \tag{23}$$

can compete with the loop–decay [12]

$$\tilde{t}_1 \to c\,\tilde{\chi}^0_{1,2}. \tag{24}$$

If also $m_{\tilde{t}_1} < m_{\tilde{\chi}^0_1} + m_b + m_W$ etc., then four–body decays [14]

$$\tilde{t}_1 \to b\,f\,\bar{f}'\,\tilde{\chi}^0_1 \tag{25}$$

have to be taken into account.

We have studied numerically the widths and branching ratios of the various sfermion decay modes. In the calculation of the stop and sbottom decay widths we have included the SUSY–QCD corrections according to [28]. In Fig. 12 we show the decay width of $\tilde{t}_1 \to b\tilde{\chi}^+_1$ as a function of $\cos\theta_{\tilde{t}}$ for $m_{\tilde{t}_1} =$ 200 GeV, $m_{\tilde{t}_2} = 420$ GeV, $\tan\beta = 4$, $M = 180$ GeV, $\mu = 360$ GeV, (gaugino–like $\tilde{\chi}^+_1$), and $M = 360$ GeV,

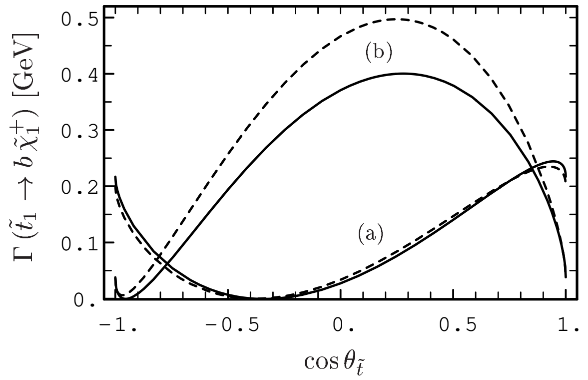

Figure 12: Decay width of $\tilde t_1$ as a function of $\cos\theta_{\tilde t}$ for $m_{\tilde t_1} = 200$ GeV, $m_{\tilde t_2} = 420$ GeV, $\tan\beta = 4$, $\{M,\, \mu\} = \{180,\, 360\}$ GeV in (a), and $\{M,\, \mu\} = \{360,\, 180\}$ GeV in (b); the dashed lines show the results at tree level, the full lines those at $\mathcal{O}(\alpha_s)$.

$\mu = 180$ GeV (higgsino–like $\tilde\chi_1^+$). If $\Gamma(\tilde t_1) \lesssim 200$ MeV $\tilde t_1$ may hadronize before decaying [30]. In Fig. 12 this is the case for a gaugino–like $\tilde\chi_1^+$ as well as for a higgsino–like one if $\cos\theta_{\tilde t} \lesssim -0.5$ (or $\cos\theta_{\tilde t} \gtrsim 0.9$).

In case that all tree–level two–body decay modes are forbidden for $\tilde t_1$, higher order decays are important for its phenomenology. In the following we study examples where three–body decay modes, Eq. (23), are the dominant ones. For fixing the parameters we choose the following procedure: in addition to $\tan\beta$ and μ we use $m_{\tilde t_1}$ and $\cos\theta_{\tilde t}$ as input parameters in the stop sector. For the sbottom (stau) sector we fix $M_{\tilde Q}, M_{\tilde D}$ and A_b (M_E, M_L, A_τ) as input parameters. (We use this mixed set of parameters in order to avoid unnaturally large values for A_b and A_τ.) Moreover, we assume for simplicity that the soft SUSY breaking parameters are equal for all generations. Note that, because of SU(2) invariance $M_{\tilde Q}$ appears in both the stop and sbottom mass matrices, see Eqs. (1)–(3). The mass of the heavier stop can thus be calculated from the above set of input parameters as:

$$m_{\tilde t_2}^2 = \frac{2M_{\tilde Q}^2 + 2\,m_Z^2 \cos 2\beta \left(\frac{1}{2} - \frac{2}{3}\sin^2\theta_W\right) + 2\,m_t^2 - m_{\tilde t_1}^2\,(1 + \cos 2\theta_{\tilde t})}{1 - \cos 2\theta_{\tilde t}} \tag{26}$$

In the sbottom (stau) sector obviously the physical quantities $m_{\tilde b_1}$, $m_{\tilde b_2}$, and $\cos\theta_{\tilde b}$ ($m_{\tilde\tau_1}, m_{\tilde\tau_2}$, $\cos\theta_{\tilde\tau}$) change with μ and $\tan\beta$.

A typical example is given in Fig. 13 where we show the branching ratios of $\tilde t_1$ as a function of $\cos\theta_{\tilde t}$. We have restricted the $\cos\theta_{\tilde t}$ range in such a way that $|A_t| \lesssim 1$ TeV to avoid color/charge breaking minima. The parameters and physical quantities are given in Table 1. In Fig. 13 a we present BR($\tilde t_1 \to b\,W^+\,\tilde\chi_1^0$), BR($\tilde t_1 \to c\,\tilde\chi_1^0$), BR($\tilde t_1 \to b\,e^+\,\tilde\nu_e$) + BR($\tilde t_1 \to b\,\nu_e\,\tilde e_L^+$), and BR($\tilde t_1 \to b\,\tau^+\,\tilde\nu_\tau$) + BR($\tilde t_1 \to b\,\nu_\tau\,\tilde\tau_1$) + BR($\tilde t_1 \to b\,\nu_\tau\,\tilde\tau_2$). Here the decay into $b\,H^+\,\tilde\chi_1^0$ is not included because for the parameters of Table 1 there is no m_A which simultaneously allows this decay and fulfils the condition $m_{h^0} \gtrsim 90$ GeV. However, in general this decay is suppressed by kinematics [13]. We have summed the branching ratios of those decays which give the the same final states after the sleptons have decayed. For example:

$$\tilde t_1 \to b\,\nu_\tau\,\tilde\tau_1 \;\to\; b\,\tau\,\nu_\tau\,\tilde\chi_1^0, \qquad \tilde t_1 \to b\,\tau\,\tilde\nu_\tau \;\to\; b\,\tau\,\nu_\tau\,\tilde\chi_1^0. \tag{27}$$

Note, that the requirement $m_{\tilde t_1} - m_b < m_{\tilde\chi_1^+}$ implies that the sleptons can only decay into the corresponding lepton plus the lightest neutralino except for a small parameter region where the decay into $\tilde\chi_2^0$ is possible. However, there this decay is negligible due to kinematics. The branching ratios for decays into $\tilde\mu_L$ or $\tilde\nu_\mu$ are not shown because they are the same as those of the decays into $\tilde e_L$ or $\tilde\nu_e$ up to very tiny mass effects. The sum of the branching ratios for the decays into $\tilde\tau_1$ and $\tilde\tau_2$ also has nearly the same

$\tan\beta$	μ	M	$m_{\tilde{\chi}^0_1}$	$m_{\tilde{\chi}^+_1}$	$m_{\tilde{\chi}^+_2}$
3	500	240	116	223	520
M_D	M_Q	A_b	$m_{\tilde{b}_1}$	$m_{\tilde{b}_2}$	$\cos\theta_{\tilde{b}}$
370	340	150	342	372	0.98
M_E	M_L	A_τ	$m_{\tilde{\tau}_1}$	$m_{\tilde{\tau}_2}$	$\cos\theta_{\tilde{\tau}}$
190	190	150	188	200	0.69
		$m_{\tilde{t}_1}$	$m_{\tilde{e}_L}$	$m_{\tilde{e}_R}$	$m_{\tilde{\nu}_\tau}$
		220	195	195	181

Table 1: Parameters and physical quantities used in Fig. 13 and 14. All masses are given in GeV.

size as $\tan\beta$ is small. BR($\tilde{t}_1 \to c\,\tilde{\chi}^0_1$) is of order 10^{-4} independent of $\cos\theta_{\tilde{t}}$ and therefore negligible. Near $\cos\theta_{\tilde{t}} = -0.3$ the decay into $b\,W^+\,\tilde{\chi}^0_1$ has a branching ratio of $\sim 100\%$. Here the $\tilde{t}_1 b \tilde{\chi}^+_1$ coupling vanishes leading to the reduction of the decays into sleptons.

In Fig. 13b the branching ratios for the decays into the different sleptons are shown. As $\tan\beta$ is small the sleptons couple mainly to the gaugino components of $\tilde{\chi}^+_1$. Therefore, the branching ratios of decays into staus, which are strongly mixed, are reduced. However, the sum of both branching ratios is nearly the same as BR($\tilde{t}_1 \to b\,\nu_e\,\tilde{e}^+_L$). The decays into sneutrinos are preferred by kinematics. The decay $\tilde{t}_1 \to b\,W^+\,\tilde{\chi}^0_1$ is dominated by top quark exchange, followed by chargino contributions. In many cases the interference term between t and $\tilde{\chi}^+_{1,2}$ is more important than the pure $\tilde{\chi}^+_{1,2}$ exchange. Moreover, we have found that the contribution from sbottom exchange is in general negligible.

In Fig. 14 we show the branching ratios of $\tilde{t}_1$ decays as a function of $\tan\beta$ for $\cos\theta_{\tilde{t}} = 0.6$ and the other parameters as above. For small $\tan\beta$ the decay $\tilde{t}_1 \to b\,W^+\,\tilde{\chi}^0_1$ is the most important one. The branching ratios for the decays into sleptons are reduced in the range $\tan\beta \lesssim 5$ because the gaugino component of $\tilde{\chi}^+_1$ decreases and its mass increases. For $\tan\beta \gtrsim 10$ the decays into the $b\,\tau\,\not{E}$ final state become more important because of the growing τ Yukawa coupling and because of kinematics ($m_{\tilde{\tau}_1}$ decreases with increasing $\tan\beta$). Here $\tilde{t}_1 \to b\,\nu_\tau\,\tilde{\tau}_1$ gives the most important contribution as can be seen in Fig. 14b. Even for large $\tan\beta$ the decay into $c\,\tilde{\chi}^0_1$ is always suppressed.

From the requirement that no two–body decays be allowed at tree level follows that $m_{\tilde{\chi}^+_1} > m_{\tilde{t}_1} - m_b$. Therefore, one expects an increase of BR($\tilde{t}_1 \to b\,W^+\,\tilde{\chi}^0_1$) if $m_{\tilde{t}_1}$ increases, because the decay into $b\,W^+\,\tilde{\chi}^0_1$ is dominated by top–quark exchange whereas for the decays into sleptons the $\tilde{\chi}^+_1$ contribution is the dominating one. In general BR($\tilde{t}_1 \to b\,W^+\,\tilde{\chi}^0_1$) is larger than 80% if $m_{\tilde{t}_1} \gtrsim 350$ GeV [13].

If the three–body decay modes are kinematically forbidden (or suppressed) four–body decays $\tilde{t}_1 \to b\,f\,\bar{f}\,\tilde{\chi}^0_1$ come into play. Depending on the MSSM parameter region, these decays can also dominate over the decay into $c\,\tilde{\chi}^0_1$. For a discussion, see [14].

We now turn to the decays of $\tilde{t}_2$. Here the bosonic decays of Eqs. 20 and 22 can play an important rôle as demonstrated in Figs. 15 and 16. In Fig. 15 we show the $\cos\theta_{\tilde{t}}$ dependence of BR($\tilde{t}_2$) for $m_{\tilde{t}_1} = 200$ GeV, $m_{\tilde{t}_2} = 420$ GeV, $M = 180$ GeV, $\mu = 360$ GeV, $\tan\beta = 4$, $M_{\tilde{D}} = 1.1\,M_{\tilde{Q}}$, $A_b = -300$ GeV, and $m_A = 200$ GeV. As can be seen, the decays into bosons can have branching ratios of several ten percent. The branching ratio of the decay into the gaugino–like $\tilde{\chi}^+_1$ is large if $\tilde{t}_2$ has a rather strong $\tilde{t}_L$ component. The decay $\tilde{t}_2 \to \tilde{t}_1 Z$ is preferred by strong mixing. The decays into $\tilde{b}_i W^+$ only occur for $|\cos\theta_{\tilde{t}}| \gtrsim 0.5$ because the sbottom masses are related to the stop parameters by our choice $M_{\tilde{D}} = 1.1\,M_{\tilde{Q}}$. Notice that BR($\tilde{t}_2 \to \tilde{b}_i W^+$) goes to zero for $|\cos\theta_{\tilde{t}}| = 1$ as in this case $\tilde{t}_2 = \tilde{t}_R$. We have chosen m_A such that decays into all MSSM Higgs bosons be possible. These decays introduce a more complicated dependence on the mixing angle, Eq. (10), because $A_t = (m^2_{\tilde{t}_1} - m^2_{\tilde{t}_2})/(2m_t) + \mu\cot\beta$ directly enters the stop–Higgs

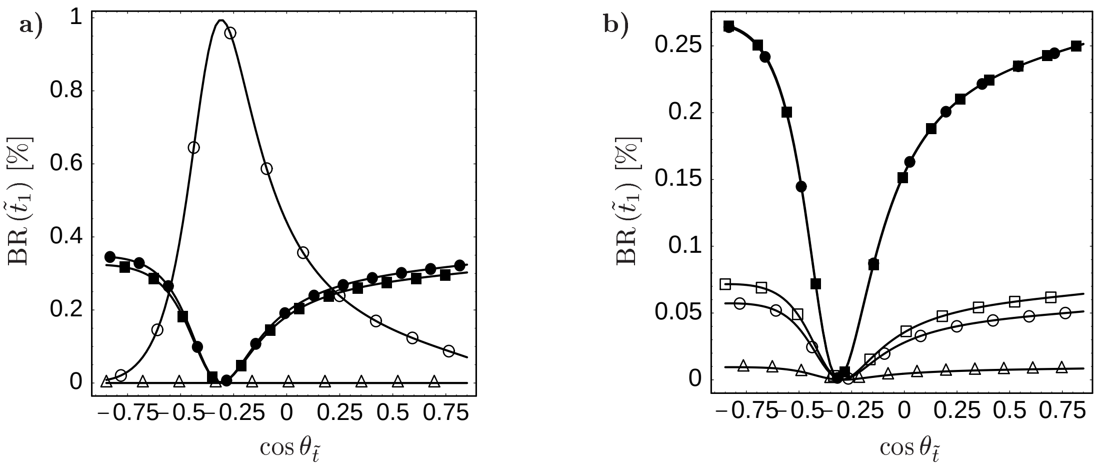

Figure 13: Branching ratios for $\tilde{t}_1$ decays as a function of $\cos\theta_{\tilde{t}}$ for $m_{\tilde{t}_1} = 220$ GeV, $\tan\beta = 3$, $\mu = 500$ GeV, and $M = 240$ GeV. The other parameters are given in Table 1. The curves in a) correspond to the transitions: $\circ$ $\tilde{t}_1 \to b\,W^+\,\tilde{\chi}^0_1$, $\triangle$ $\tilde{t}_1 \to c\tilde{\chi}^0_1$, $\blacksquare$ $(\tilde{t}_1 \to b\,e^+\,\tilde{\nu}_e) + (\tilde{t}_1 \to b\,\nu_e\,\tilde{e}^+_L)$, and $\bullet$ $(\tilde{t}_1 \to b\,\tau^+\,\tilde{\nu}_\tau) + (\tilde{t}_1 \to b\,\nu_\tau\,\tilde{\tau}_1) + (\tilde{t}_1 \to b\,\nu_\tau\,\tilde{\tau}_2)$. The curves in b) correspond to the transitions: $\circ$ $\tilde{t}_1 \to b\,\nu_e\,\tilde{e}^+_L$, $\square$ $\tilde{t}_1 \to b\,\nu_\tau\,\tilde{\tau}_1$, $\triangle$ $\tilde{t}_1 \to b\,\nu_\tau\,\tilde{\tau}_2$, $\blacksquare$ $\tilde{t}_1 \to b\,e^+\,\tilde{\nu}_e$, and $\bullet$ $\tilde{t}_1 \to b\,\tau^+\,\tilde{\nu}_\tau$.

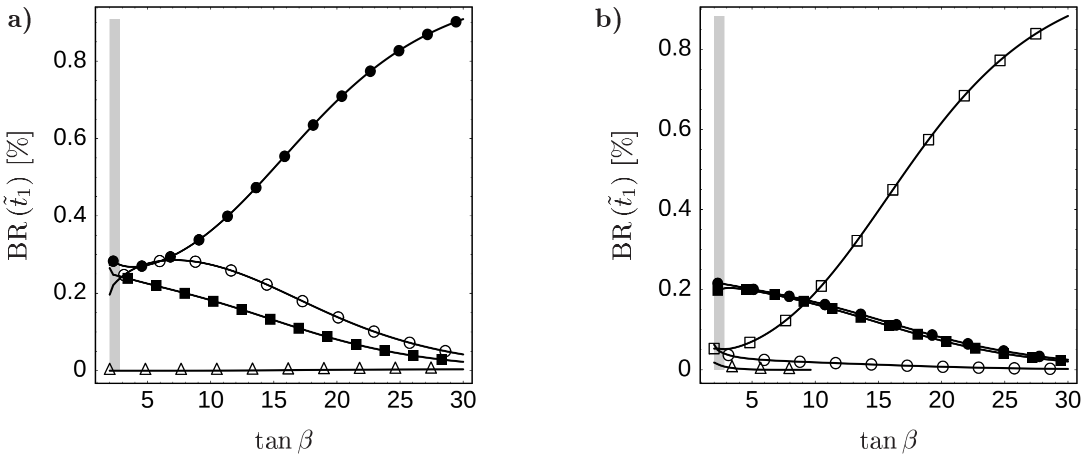

Figure 14: Branching ratios for $\tilde{t}_1$ decays as a function of $\tan\beta$ for $m_{\tilde{t}_1} = 220$ GeV, $\mu = 500$ GeV, $\cos\theta_{\tilde{t}} = 0.25$ and $M = 240$ GeV. The other parameters are given in Table 1. The curves in a) correspond to the transitions: $\circ$ $\tilde{t}_1 \to b\,W^+\,\tilde{\chi}^0_1$, $\triangle$ $\tilde{t}_1 \to c\tilde{\chi}^0_1$, $\blacksquare$ $(\tilde{t}_1 \to b\,e^+\,\tilde{\nu}_e) + (\tilde{t}_1 \to b\,\nu_e\,\tilde{e}^+_L)$, and $\bullet$ $(\tilde{t}_1 \to b\,\tau^+\,\tilde{\nu}_\tau) + (\tilde{t}_1 \to b\,\nu_\tau\,\tilde{\tau}_1) + (\tilde{t}_1 \to b\,\nu_\tau\,\tilde{\tau}_2)$. The curves in b) correspond to the transitions: $\circ$ $\tilde{t}_1 \to b\,\nu_e\,\tilde{e}^+_L$, $\square$ $\tilde{t}_1 \to b\,\nu_\tau\,\tilde{\tau}_1$, $\triangle$ $\tilde{t}_1 \to b\,\nu_\tau\,\tilde{\tau}_2$, $\blacksquare$ $\tilde{t}_1 \to b\,e^+\,\tilde{\nu}_e$, and $\bullet$ $\tilde{t}_1 \to b\,\tau^+\,\tilde{\nu}_\tau$. In gray area $m_{h^0} < 90$ GeV.

couplings. Here notice also the dependence on the sign of $\cos\theta_{\tilde{t}}$.

Figure 16 shows the branching ratios of $\tilde{t}_2$ decays as a function of $m_{\tilde{t}_2}$ for $\cos\theta_{\tilde{t}} = -0.66$ and the other parameters as in Fig. 15. Again we compare the fermionic and bosonic decay modes. While for a rather light $\tilde{t}_2$ the decay into $b\tilde{\chi}^+_1$ is the most important one, with increasing mass difference $m_{\tilde{t}_2} - m_{\tilde{t}_1}$ the decays into bosons, especially $\tilde{t}_2 \to \tilde{t}_1 Z$, become dominant.

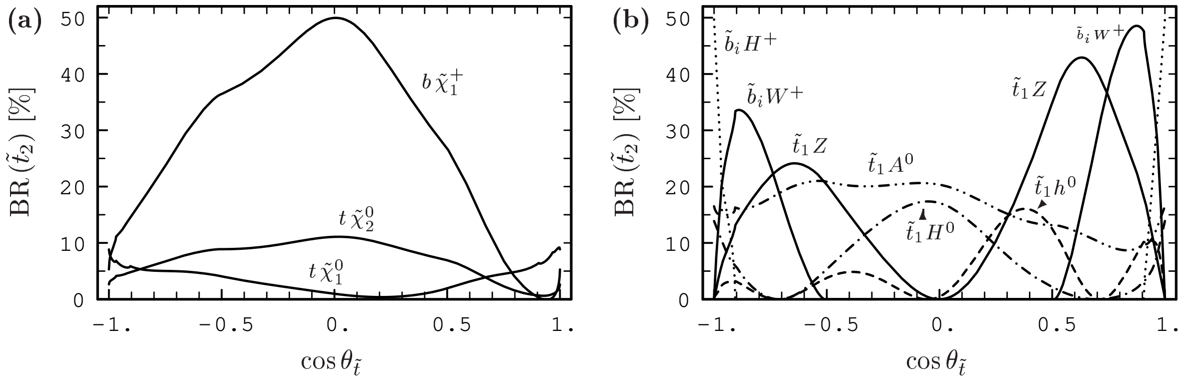

Figure 15: Branching ratios of $\tilde{t}_2$ decays at $\mathcal{O}(\alpha_s)$ as a function of $\cos\theta_{\tilde{t}}$ for $m_{\tilde{t}_1} = 200$ GeV, $m_{\tilde{t}_2} = 420$ GeV, $M = 180$ GeV, $\mu = 360$ GeV, $\tan\beta = 4$, $M_{\tilde{D}} = 1.1\, M_{\tilde{Q}}$, $A_b = -300$ GeV, and $m_A = 200$ GeV; the fermionic decays are shown in (a) and the bosonic ones in (b).

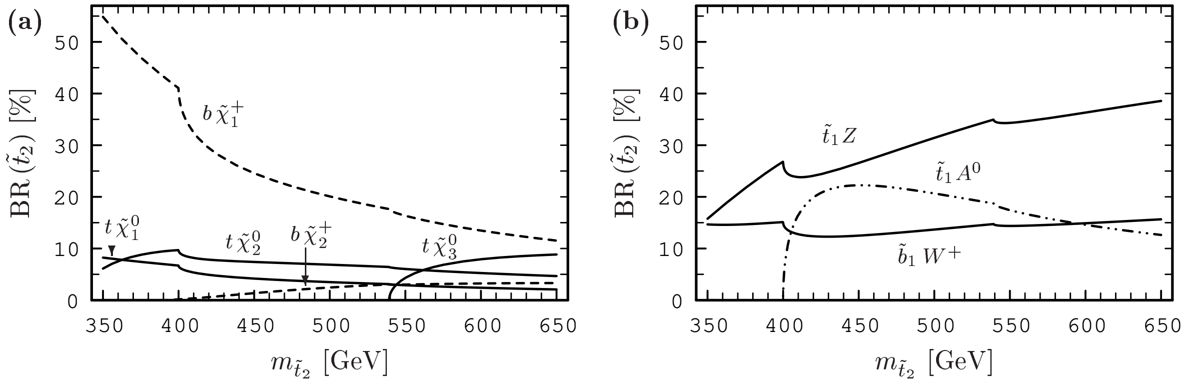

Figure 16: Branching ratios of $\tilde{t}_2$ decays at $\mathcal{O}(\alpha_s)$ as a function of $m_{\tilde{t}_2}$ for $m_{\tilde{t}_1} = 200$ GeV, $\cos\theta_{\tilde{t}} = -0.66$, $M = 180$ GeV, $\mu = 360$ GeV, $\tan\beta = 4$, $M_{\tilde{D}} = 1.1\, M_{\tilde{Q}}$, $A_b = -300$ GeV, and $m_A = 200$ GeV; the fermionic decays are shown in (a) and the bosonic ones in (b).

Concerning the decays of $\tilde{b}_1$ and $\tilde{b}_2$ we found that the allowed range of e.g., $m_{\tilde{b}_i}$ or $\cos\theta_{\tilde{b}}$ is very restricted, once the other parameters are fixed. Therefore, we do not show figures of sbottom branching ratios. In general, however, for $\tilde{b}_1$ the decays into $b\tilde{\chi}_1^0$ and $b\tilde{\chi}_2^0$ are important for gaugino–like $\tilde{\chi}_{1,2}^0$ because the decay $\tilde{b}_1 \to t\tilde{\chi}_1^-$ is kinematically suppressed. For $\tilde{b}_2$, decays into Z and/or neutral Higgs bosons are important if the mass difference $m_{\tilde{b}_2} - m_{\tilde{b}_1}$ is large enough. This may well be the case for large $\tan\beta$ and/or large μ. If strong mixing in the stop sector leads to a light $\tilde{t}_1$ then also the decays $\tilde{b}_i \to \tilde{t}_1 W^-\,(H^-)$ can have large branching ratios. For $m_{\tilde{b}_1} = 284$ GeV, $m_{\tilde{b}_2} = 345$ GeV, $\cos\theta_{\tilde{b}} = 0.84$, $M = 180$ GeV, $\mu = 360$ GeV, and $\tan\beta = 10$ for instance (taking $M_{\tilde{U}} = 0.9\, M_{\tilde{Q}}$ and $A_t = -375$ GeV to fix the stop sector), we find BR$(\tilde{b}_1 \to b\tilde{\chi}_1^0) = 16\%$, BR$(\tilde{b}_1 \to b\tilde{\chi}_2^0) = 58\%$, BR$(\tilde{b}_1 \to \tilde{t}_1 W^-) = 26\%$, and BR$(\tilde{b}_2 \to b\tilde{\chi}_1^0) = 10\%$, BR$(\tilde{b}_2 \to b\tilde{\chi}_2^0) = 15\%$, BR$(\tilde{b}_2 \to \tilde{t}_1 W^-) = 74\%$. More details and plots on stop and sbottom decays can be found in [5, 16, 31, 32].

For the discussion of $\tilde{\tau}_{1,2}$ and $\tilde{\nu}_\tau$ decays we first consider the scenario of Fig. 2 where all particles are relatively light and have only fermionic decay modes. In Fig. 17 we show the branching ratios of $\tilde{\tau}_1$ and $\tilde{\tau}_2$ decays as a function of $\cos\theta_{\tilde{\tau}}$ for $m_{\tilde{\tau}_1} = 156$ GeV, $m_{\tilde{\tau}_2} = 180$ GeV, $M = 120$ GeV, $\mu = 300$ GeV, and $\tan\beta = 4$. In this case, decays into $\tilde{\chi}_1^0 \sim \tilde{B}$, $\tilde{\chi}_2^0 \sim \tilde{W}^3$, and $\tilde{\chi}_1^\pm \sim \tilde{W}^\pm$ are kinematically allowed.

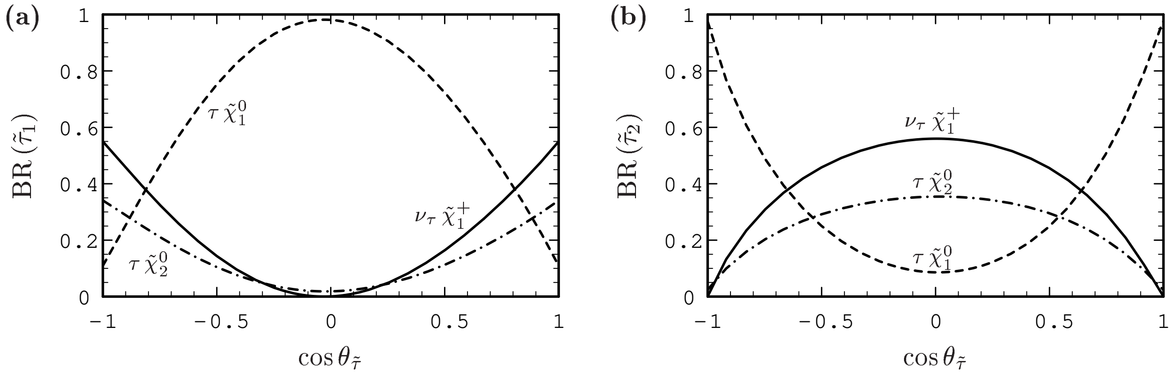

Figure 17: Branching ratios of $\tilde{\tau}_1$ (a) and $\tilde{\tau}_2$ (b) decays as a function of $\cos\theta_{\tilde{\tau}}$ for $m_{\tilde{\tau}_1} = 156$ GeV, $m_{\tilde{\tau}_2} = 180$ GeV, $M = 120$ GeV, $\mu = 300$ GeV, and $\tan\beta = 4$.

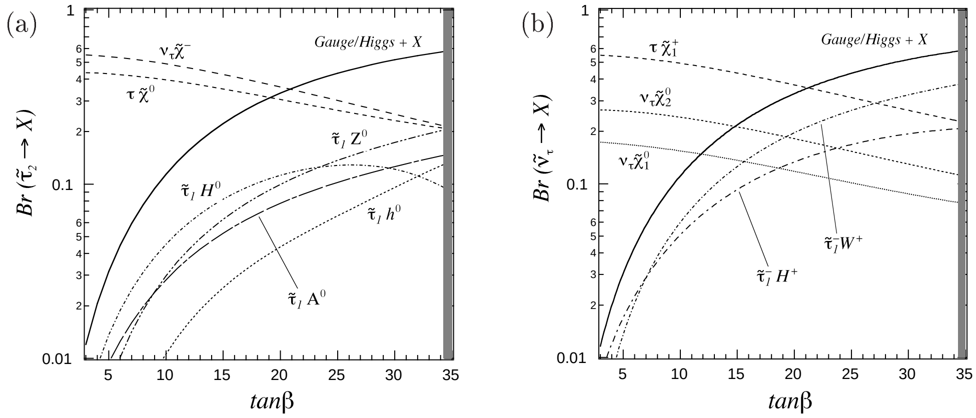

Figure 18: $\tan\beta$ dependence of $\tilde{\tau}_2$ (a) and $\tilde{\nu}_\tau$ (b) decay branching ratios for $m_{\tilde{\tau}_1} = 250$ GeV, $m_{\tilde{\tau}_2} = 500$ GeV, $m_{\tilde{\tau}_L} < m_{\tilde{\tau}_R}$, $A_\tau = 800$ GeV and $\mu = 1000$ GeV; the other parameters are: $M = 300$ GeV, $m_A = 150$ GeV, and $M_{\tilde{Q}} = M_{\tilde{U}} = M_{\tilde{D}} = A_t = A_b = 500$ GeV.

Therefore, for $\cos\theta_{\tilde{\tau}} \sim 0$ $\tilde{\tau}_1$ decays predominately into $\tau\tilde{\chi}^0_1$ while for $|\cos\theta_{\tilde{\tau}}| \sim 1$ it mainly decays into $\tau\tilde{\chi}^0_2$ and $\tilde{\nu}_\tau\tilde{\chi}^-_1$. $\tilde{\tau}_2$ shows the opposite behaviour. For the $\tilde{\nu}_\tau$ decays we obtain $\mathrm{BR}(\tilde{\nu}_\tau \to \nu\tilde{\chi}^0_1) = 32\%$, $\mathrm{BR}(\tilde{\nu}_\tau \to \nu\tilde{\chi}^0_2) = 17\%$, and $\mathrm{BR}(\tilde{\nu}_\tau \to \tau\tilde{\chi}^+_1) = 51\%$ for $m_{\tilde{\nu}_\tau} = 148$ GeV and the other parameters as in Fig. 2. This means that at least 1/3 of the events are invisible.

In case of a large mass splitting $m_{\tilde{\tau}_2} - m_{\tilde{\tau}_1}$, $\tilde{\tau}_i$ and $\tilde{\nu}_\tau$ can also decay into gauge or Higgs bosons. This is especially the case if $\tan\beta$, A_τ and μ are large. As an example, Fig. 18 shows the branching ratios of $\tilde{\tau}_2$ and $\tilde{\nu}_\tau$ decays as a function of $\tan\beta$ for $m_{\tilde{\tau}_1} = 250$ GeV, $m_{\tilde{\tau}_2} = 500$ GeV, $m_{\tilde{\tau}_L} < m_{\tilde{\tau}_R}$, $A_\tau = 800$ GeV and $\mu = 1000$ GeV, $M = 300$ GeV, and $m_A = 150$ GeV. ("Gauge/Higgs + X" refers to the sum of the gauge and Higgs boson modes.) As can be seen, with increasing $\tan\beta$ the bosonic decay modes become dominant. See [33] for more details.

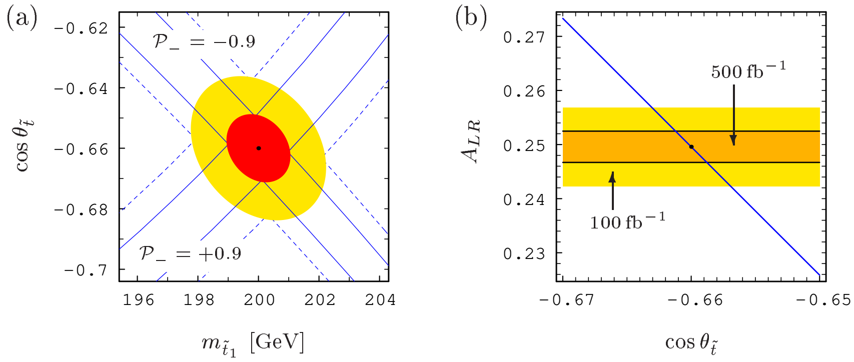

Figure 19: (a) Error bands and 68% CL error ellipse for determining $m_{\tilde t_1}$ and $\cos\theta_{\tilde t}$ from cross section measurements; the dashed lines are for $\mathcal{L} = 100$ fb^{-1} and the full lines for $\mathcal{L} = 500$ fb^{-1}. (b) Error bands for the determination of $\cos\theta_{\tilde t}$ from A_{LR}. In both plots $m_{\tilde t_1} = 200$ GeV, $\cos\theta_{\tilde t} = -0.66$, $\sqrt{s} = 500$ GeV, $\mathcal{P}_- = \pm 0.9$, $\mathcal{P}_+ = 0$, and the other parameters as in Fig. 1.

4 Parameter determination

We next estimate the precision one may obtain for the parameters of the $\tilde t$ sector from cross section measurements. We use the parameter point of Fig. 1, i.e. $m_{\tilde t_1} = 200$ GeV, $m_{\tilde t_2} = 420$ GeV, $\cos\theta_{\tilde t} = -0.66$, etc. as an illustrative example: For 90% left–polarized electrons (and unpolarized positrons) we have $\sigma_L(\tilde t_1 \bar{\tilde t}_1) = 44.88$ fb, including SUSY–QCD, Yukawa coupling, and ISR corrections. For 90% right–polarized electrons we have $\sigma_R(\tilde t_1 \bar{\tilde t}_1) = 26.95$ fb. Assuming that M, μ, $\tan\beta$, and m_A will be known from other measurements with a precision of about 10%, we estimate the theoretical uncertanity of the production cross sections to be $\lesssim 1\%$. According to the Monte Carlo study of [34] one can expect to measure these cross sections with a statistical error of $\Delta\sigma_L = 2.1\,\%$ and $\Delta\sigma_R = 2.8\,\%$ in case of an integrated luminosity of $\mathcal{L} = 500$ fb^{-1} (i.e. $\mathcal{L} = 250$ fb^{-1} for each polarization). Scaling these values to $\mathcal{L} = 100$ fb^{-1} leads to $\Delta\sigma_L = 4.7\,\%$ and $\Delta\sigma_R = 6.3\,\%$. Figure 19a shows the corresponding error bands and error ellipses in the $m_{\tilde t_1}$–$\cos\theta_{\tilde t}$ plane. The resulting errors on the stop mass and mixing angle are: $\Delta m_{\tilde t_1} = 2.2$ GeV, $\Delta\cos\theta_{\tilde t} = 0.02$ for $\mathcal{L} = 100$ fb^{-1} and $\Delta m_{\tilde t_1} = 1.1$ GeV, $\Delta\cos\theta_{\tilde t} = 0.01$ for $\mathcal{L} = 500$ fb^{-1}. With the additional use of a 60% polarized e^+ beam these values can still be improved by $\sim 25\%$. At $\sqrt{s} = 800$ GeV also $\tilde t_2$ can be produced: $\sigma(\tilde t_1 \bar{\tilde t}_2 + \mathrm{c.c.}) = 8.75\,$fb for $\mathcal{P}_- = -0.9$ and $\mathcal{P}_+ = 0$. If this cross section can be measured with a precision of $6\,\%$ this leads to $m_{\tilde t_2} = 420 \pm 8.9$ GeV (again, we took into account a theoretical uncertainity of 1%).[2] With $\tan\beta$ and μ known from other measurements this then allows one to determine the soft SUSY breaking parameters of the stop sector. Assuming $\tan\beta = 4 \pm 0.4$ leads to $M_{\tilde Q} = 298 \pm 8$ GeV and $M_{\tilde U} = 264 \pm 7$ GeV for $\mathcal{L} = 500\,$fb^{-1}. In addition, assuming $\mu = 800 \pm 80$ GeV we get $A_t = 587 \pm 35$ (or -187 ± 35) GeV. The ambiguity in A_t exists because the sign of $\cos\theta_{\tilde t}$ can hardly be determined from cross section measurements. This may, however, be possible from measuring decay branching ratios or the stop–Higgs couplings.

A different method to determine the sfermion mass is to use kinematical distributions. This was studied in [35] for squarks of the 1st and 2nd generation. It was shown that, by fitting the distribution of the minimum kinematically allowed squark mass, it is possible to determine $m_{\tilde q}$ with high precision. To be precise, [35] concluded that at $\sqrt{s} = 500$ GeV, $m_{\tilde q} \sim 200$ GeV could be determined with an error of $\lesssim 0.5\%$ using just $20\,$fb^{-1} of data (assuming that all squarks decay via $\tilde q \to q \tilde\chi^0_1$ and $m_{\tilde\chi^0_1}$ is known). The influence of radiative effects on this method has been studied in [36]. Taking into account initial

[2]Here note that $\tilde t_1 \bar{\tilde t}_1$ is produced at $\sqrt{s} = 800$ GeV with an even higher rate than at $\sqrt{s} = 500$ GeV. One can thus improve the errors on $m_{\tilde t_1}$, $m_{\tilde t_2}$, and $\cos\theta_{\tilde t}$ by combining the information obtained at different energies. However, this is beyond the scope of this study.

state radiation of photons and gluon radiation in the production and decay processes it turned out that a mass of $m_{\tilde{q}} = 300$ GeV could be determined with an accuracy of $\lesssim 1\%$ with $50\,\mathrm{fb}^{-1}$ of data. (This result will still be affected by the error on the assumed $m_{\tilde{\chi}^0_1}$, hadronization effects, and systematic errors.) Although the analysis of [35, 36] was performed for squarks of the 1st and 2nd generation, the method is also applicable to the 3rd generation.

For the determination of the mixing angle, one can also make use of the left–right asymmetry A_{LR}, Eq. (16). This quantity is of special interest because kinematic effects and uncertainities in experimental efficiencies largely drop out. At $\sqrt{s} = 500$ GeV we get $A_{LR}(e^+e^- \to \tilde{t}_1\bar{\tilde{t}}_1) = 0.2496$ for the parameter point of Fig. 1 and 90% polarized electrons. Taking into account experimental errors as determined in [34], a theoretical uncertanity of 1%, and $\delta P/P = 10^{-2}$ we get $\Delta A_{LR} = 2.92\%$ (1.16%) for $\mathcal{L} = 100\,\mathrm{fb}^{-1}$ ($500\,\mathrm{fb}^{-1}$). This corresponds to $\Delta\cos\theta_{\tilde{t}} = 0.0031$ (0.0012). This is most likely the most precise method to determine the stop mixing angle. The corresponding error bands are shown in Fig. 19 b.

A Monte Carlo study of stau production, with $\tilde{\tau}_1 \to \tau\tilde{\chi}^0_1$, was performed in [37]. They also give a method for the parameter determination concluding that $m_{\tilde{\tau}_1}$ and $\theta_{\tilde{\tau}}$ could be measured with an accurracy of $\mathcal{O}(1\%)$.

5 Comparison with LHC and Tevatron

In this section we briefly discuss the possibilites of detecting (light) stops, sbottoms, and staus at the LHC or Tevatron. At hadron colliders, stops and sbottoms are produced in pairs via gluon–gluon fusion or $q\bar{q}$ annihilation. They are also produced singly in gluon–quark interactions. At leading order, the production cross sections depend only on the masses of the particles produced. The NLO corrections introduce a dependence on the other MSSM parameters of $\mathcal{O}(1\%)$ [38]. In addition, stops and sbottoms can be produced in cascade decays e.g., $\tilde{g} \to t\tilde{t}_i$, $\tilde{g} \to b\tilde{b}_j$ with $\tilde{b}_j \to \tilde{t}_i W^-$, $\tilde{q} \to q\bar{q}\tilde{\chi}^0_j$ with $\tilde{\chi}^0_j \to t\tilde{t}_i$ etc.

At the LHC one is, in general, sensitive to squark masses up to ~ 2 TeV [39, 40]. Searches for stops, however, suffer from an overwhelming background from top quarks, which makes the analysis very difficult. Here notice that e.g., $\sigma(pp \to \tilde{t}_1\bar{\tilde{t}}_1) \sim \frac{1}{10}\sigma(pp \to t\bar{t})$ for $m_{\tilde{t}_1} \sim m_t$ and $\sigma(pp \to \tilde{t}_1\bar{\tilde{t}}_1) \sim \frac{1}{100}\sigma(pp \to t\bar{t})$ for $m_{\tilde{t}_1} \sim 300$ GeV. Therefore, [8] concluded that it is 'extremely difficult' to extract a $\tilde{t}$ signal if the SUSY parameters are [similar to] those of LHC Point 4, i.e. $m_0 = 800$ GeV, $m_{1/2} = 200$ GeV, $A = 0$, $\tan\beta = 10$, and $\mu > 0$, leading to $m_{\tilde{t}_1} = 594$ GeV and $m_{\tilde{g}} = 582$ GeV. The situation is more promising for LHC Point 5, i.e. $m_0 = 100$ GeV, $m_{1/2} = 300$ GeV, $A = 300$ GeV, $\tan\beta = 2.1$, and $\mu > 0$, leading to $m_{\tilde{t}_1} = 490$ GeV and $m_{\tilde{g}} = 770$ GeV. In this case $m_{\tilde{t}_1}$ can be determined with an accuracy of $\sim 10\%$ [9]. However, no information on $\theta_{\tilde{t}}$ is obtained. More importantly, in [7] it turned out that a light $\tilde{t}_1$ with $m_{\tilde{t}_1} \lesssim 250$ GeV is extremely difficult to observe at LHC.

Such a light $\tilde{t}_1$ could, in principle, be within the reach of the Tevatron Run II. A rather complete study of the Tevatron potential for stop searches was performed in [11]. It turned out that the reach in $m_{\tilde{t}_1}$ depends very much on the decay channel(s) and kinematics and, of course, on the luminosity. For example, for $\tilde{t}_1 \to b\,\tilde{\chi}^+_1$ with $\mathcal{L} = 2\,\mathrm{fb}^{-1}$, it is not possible to go beyond the LEP2 limit of $m_{\tilde{t}_1} \gtrsim 100$ GeV. With $\mathcal{L} = 20\,\mathrm{fb}^{-1}$ the reach extends up to $m_{\tilde{t}_1} = 175$ (212) GeV if $m_{\tilde{\chi}^+_1} = 130$ (100) GeV. If $\tilde{t}_1$ decays into $c\tilde{\chi}^0_1$, with $\mathcal{L} = 2\,\mathrm{fb}^{-1}$ one can exclude $m_{\tilde{t}_1} \lesssim 180$ GeV provided $m_{\tilde{\chi}^0_1} \sim 100$; with $\mathcal{L} = 20\,\mathrm{fb}^{-1}$ one can exclude $m_{\tilde{t}_1} \lesssim 225$ GeV if $m_{\tilde{\chi}^0_1} \lesssim 135$ GeV. Notice, however, that no limit on $m_{\tilde{t}_1}$ can be obtained with $\mathcal{L} = 2$ (20) fb^{-1} if $m_{\tilde{\chi}^0_1} \gtrsim 110$ (140) GeV or if $m_{\tilde{t}_1} - m_{\tilde{\chi}^0_1} \lesssim 15$ GeV. If $m_{\tilde{\chi}^0_1} \lesssim m_{\tilde{t}_1} - m_b - m_W$ the decay $\tilde{t}_1 \to bW\tilde{\chi}^0_1$ becomes relevant and one can hardly exceed the limits from LEP searches, even not with $\mathcal{L} = 20\,\mathrm{fb}^{-1}$. Similar results have been obtained for $\tilde{t}_1$ three–body decays into sleptons.

The authors of [11] also studied the search for light sbottoms at the Tevatron Run II concentrating on the decay $\tilde{b}_1 \to b\tilde{\chi}^0_1$ within mSUGRA. They conclude that with $2\,\mathrm{fb}^{-1}$ of data the reach is $m_{\tilde{b}_1} \lesssim 200$ (155) GeV for $m_{\tilde{\chi}^0_1} \simeq 70$ (100) GeV. With $20\,\mathrm{fb}^{-1}$ one is sensitive to $m_{\tilde{b}_1} \lesssim 260$ (200) GeV for $m_{\tilde{\chi}^0_1} \simeq 70$ (100) GeV. Moreover, their analysis requires a mass difference of $m_{\tilde{b}_1} - m_{\tilde{\chi}^0_1} \gtrsim 30$ GeV. The higher reach compared to $\tilde{t}_1 \to c\tilde{\chi}^0_1$ is due to the higher tagging efficiency of b's. Similarly, also at the LHC the search for sbottoms is, in general, expected to be easier than that for stops. There are, however, cases where the analysis is very difficult, see e.g. [8].

The search for staus crucially depends on the possibility of τ identification. At hadron colliders, $\tilde{\tau}$'s are produced directly via the Drell–Yan process mediated by γ, Z or W exchange in the s–channel. They can also be produced in decays of charginos or neutralinos originating from squark and gluino cascade decays e.g., $\tilde{q} \to q'\tilde{\chi}^\pm_j$ with $\tilde{\chi}^\pm_j \to \tilde{\tau}^\pm_i \nu_\tau$ or $\tilde{\chi}^\pm_j \to \tilde{\nu}_\tau \tau^\pm$. At Tevatron energies, W pair production is the dominant background, while $t\bar{t}$ events, with the b jets being too soft to be detected, are the main background at the LHC. SUSY background mainly comes from $\tilde{\chi}^\pm\tilde{\chi}^\mp$ production followed by leptonic decays. The Drell–Yan production has a low cross section, and it is practically impossible to extract the signal from the SM background (SUSY background is less important). The situation is different if chargino and neutralino decays into staus have a large branching ratio. As pointed out in [41, 42, 44] this is the case for large $\tan\beta$ where the tau Yukawa coupling becomes important. In [42, 43, 40] the decays $\tilde{\chi}^\pm_1 \to \tilde{\tau}_1 \nu_\tau$ and $\tilde{\chi}^0_2 \to \tilde{\tau}_1 \tau$ ($\tilde{\tau}_1 \to \tau\tilde{\chi}^0_1$) with the τ's decaying hadronically have been studied. In [44, 45], the dilepton mass spectrum of final states with $e^+e^-/\mu^+\mu^-/e^\pm\mu^\mp + E_T^{miss} + jets$ has been used to identify $\tilde{\tau}_1$ in the decay chain $\tilde{\chi}^0_2 \to \tilde{\tau}_1\tau \to \tilde{\chi}^0_1\tau^+\tau^-$ with $\tau \to e\,(\mu) + \nu_{e\,(\mu)} + \nu_\tau$. It turned out that $\tilde{\tau}_1$ with $m_{\tilde{\tau}_1} \lesssim 350$ GeV ought to be discovered at the LHC if $m_{\tilde{\tau}_1} < m_{\tilde{\chi}^0_2}$ and $\tan\beta \gtrsim 10$.

From this one can conclude that there exist MSSM parameter regions for which (light) sfermions of the 3rd generation may escape detection at both the Tevatron and the LHC. This is in particular the case for $\tilde{t}_1$ if $m_{\tilde{t}_1} \lesssim 250$ GeV, and for $\tilde{\tau}_1$ if $\tan\beta \lesssim 10$ (or $m_{\tilde{\tau}_1} > m_{\tilde{\chi}^0_2}$). In these cases, an e^+e^- Linear Collider would not only allow for precision measurements but even serve as a discovery machine.

6 Summary

In this contribution we discussed the phenomenology of stops, sbottoms, τ–sneutrinos, and staus at an e^+e^- Linear Collider with $\sqrt{s} = 0.5 - 1$ TeV. We presented numerical predictions within the Minimal Supersymmetric Standard Model for the production cross sections and the decay rates of these particles, and analyzed their SUSY parameter dependence. Beam polarization turned out to be a very useful tool: Firstly, the dependence of the production cross sections on the sfermion mixing angles is significantly stronger if polarized beams are used. Secondly, one could enhance the production of $\tilde{f}_2$ pairs and reduce at the same time the production of $\tilde{f}_1$ pairs or vice versa. In such a case a better separation of the two mass eigenstates is possible. Concerning the decays, we showed that squarks and sleptons of the 3rd generation can have quite complex decay patterns. In particular, we discussed higher–order decays of $\tilde{t}_1$. Moreover, we showed that for $\tilde{t}$, $\tilde{b}$, $\tilde{\tau}$ and $\tilde{\nu}_\tau$ decays into lighter sfermions plus gauge or Higgs bosons can have large branching ratios. We also made a case study for the determination of the MSSM parameters of the $\tilde{t}$ sector, showing that a precision of few percent may be achieved at the Linear Collider. Comparing with LHC and Tevatron, a light $\tilde{t}_1$ ($m_{\tilde{t}_1} \lesssim 250$ GeV) may escape detection at the hadron colliders. In this case it will be discovered at a Linear Collider with $\sqrt{s} = 500$ GeV. Also the detection of $\tilde{\tau}$'s is possible at the LHC only in a quite limited parameter range whereas it should be no problem at the Linear Collider.

Acknowledgements

We thank the organizers of the various ECFA/DESY meetings for creating an intimate and inspiring working atmosphere. We also thank H.U. Martyn and L. Rurua for fruitful discussions and suggestions. This work was supported in part by the "Fonds zur Förderung der Wissenschaftlichen Forschung of Austria", project no. P13139-PHY. W.P. is supported by the Spanish "Ministerio de Educacion y Cultura" under the contract SB97-BU0475382, by DGICYT grant PB98-0693, and by the TMR contract ERBFMRX-CT96-0090.

References

[1] H.P. Nilles, Phys. Rep. 110 (1984) 1; H.E. Haber, G.L. Kane, Phys. Rep. 117 (1985) 75.

[2] J. Ellis, S. Rudaz, Phys. Lett. B128 (1983) 248.

[3] G. Altarelli, R. Rückl, Phys. Lett. B144 (1984) 126; I. Bigi, S. Rudaz, Phys. Lett. B153 (1985) 335.

[4] M. Drees, M. M. Nojiri, Nucl. Phys. B 369 (1992) 54.

[5] A. Bartl, W. Majerotto, W. Porod, Z. Phys. C64 (1994) 499.

[6] E. Accomando et al., Phys. Rep. 299 (1998) 1.

[7] U. Dydak, diploma thesis, Vienna 1996; CMS TN/96-022.

[8] F. Gianotti, ATLAS Internal Note PHYS-No-110 (1997).

[9] G. Polesello, L. Poggioli, E. Richter–Wąs, J. Söderqvist, ATLAS Internal Note PHYS-No-111 (1997).

[10] R. Arnowitt et al., in *Report of the tev 2000 Study Group*, eds. D. Amidei and R. Brock, FERMILAB-PUB-96/082 (1996).

[11] R. Demina, J. D. Lykken, K. T. Matchev, A. Nomerotski, hep-ph/9910275.

[12] K. I. Hikasa, M. Kobayashi, Phys. Rev. D36 (1987) 724.

[13] W. Porod, T. Wöhrmann, Phys. Rev. D55 (1997) 2907; W. Porod, Phys. Rev. D59 (1999) 095009.

[14] C. Boehm, A. Djouadi, Y. Mambrini, hep-ph/9907428.

[15] J. F. Gunion, H. E. Haber, Nucl. Phys. B 272 (1986) 1

[16] S. Kraml, doctoral thesis, TU Vienna 1999, hep-ph/9903257.

[17] A. Bartl, H. Eberl, S. Kraml, W. Majerotto, W. Porod, A. Sopczak, Z. Phys. C76 (1997) 76.

[18] H. Eberl, S. Kraml, Fortran program CALVIN, `http://wwwhephy.oeaw.ac.at/kraml/lib/`

[19] M. Drees, K.I. Hikasa, Phys. Lett. B252 (1990) 127; W. Beenakker, R. Höpker, P.M. Zerwas, Phys. Lett. B349 (1995) 463; K.I. Hikasa and J. Hisano, Phys. Rev. D54 (1996) 1908.

[20] H. Eberl, A. Bartl, W. Majerotto, Nucl. Phys. B472 (1996) 481.

[21] E.A. Kuraev, V.S. Fadin, Sov. J. Nucl. Phys. 41 (1985) 3; M.E. Peskin, in *Physics at the 100 GeV Mass Scale*, 17th SLAC Summer Institute, 1989.

[22] H. Eberl, S. Kraml, W. Majerotto, JHEP 9905 (1999) 016.

[23] I.I. Bigi, V.S. Fadin, V. Khoze, Nucl. Phys. B377 (1992) 461.

[24] M. Antonelli, N. Fabiano, hep-ph/9906535.

[25] R. Brinkmann (for the TESLA Collaboration), DESY-TESLA-99-15, Sep 1999.

[26] C. Baltay, talk at the 2nd ECFA/DESY Study on Physics and Detectors for a Linear Electron–Positron Collider, 16–18 Oct 1999, Obernai, France.

[27] K. Inoue, A. Kakuto, H. Komatsu, S. Takeshita, Prog. Theor. Phys. 68 (1982) 927; M. Drees, S. P. Martin, hep-ph/9504324.

[28] K. I. Hikasa, Y. Nakamura, Z. Phys. C70 (1996) 139, E: C71 (1996) 356; S. Kraml et al., Phys. Lett. B386 (1996) 175; A. Djouadi, W. Hollik, C. Jünger, Phys. Rev. D55 (1997) 6975; W. Beenakker et al., Z. Phys. C75 (1997) 349; A. Bartl et al., Phys. Lett. B 419 (1998) 243; A. Arhib et al., Phys. Rev. D57 (19998) 5860; A. Bartl et al., Phys. Rev. D59 (1999) 115007.

[29] J. Guash, W. Hollik, J. Solà, Phys. Lett. B437 (1998) 88.

[30] M. Drees, O.J.P. Éboli, Eur. Phys. J. C10 (1999) 337.

[31] A. Bartl, H. Eberl, K. Hidaka, S. Kraml, T. Kon, W. Majerotto, W. Porod, Y. Yamada, Phys. Lett. B435 (1998) 118.

[32] W. Porod, doctoral thesis, Univ. Vienna 1997, hep-ph/9804208.

[33] A. Bartl, H. Eberl, K. Hidaka, S. Kraml, T. Kon, W. Majerotto, W. Porod, Y. Yamada, Phys. Lett. B460 (1999) 157.

[34] M. Berggren, R. Keranen, H. Nowak, A. Sopczak, hep-ph/9911345.

[35] J. L. Feng, D. E. Finnell, Phys. Rev. D49 (1994) 2369.

[36] M. Drees, O.J.P. Éboli, R. Godbole, S. Kraml, contribution to the Les Houches workshop "Physics at TeV Colliders", Les Houches, France, 8-18 June 1999.

[37] M. M. Nojiri, K. Fujii, T. Tsukamoto, Phys. Rev. D54 (1994) 1996.

[38] W. Beenakker et al., Nucl. Phys. B515 (1998) 3.

[39] CMS collaboration (S. Abdullin et al.), CMS Note 1998/006, hep-ph/9806366.

[40] ATLAS collaboration, CERN/LHCC/99-15, ATLAS TDR 15 (1999).

[41] H. Baer, C. Chen, M. Drees, F. Paige, X. Tata, Phys. Rev. Lett. 79 (1997) 986.

[42] H. Baer, C. Chen, M. Drees, F. Paige, X. Tata, Phys. Rev. D58 (1998) 075008.

[43] H. Baer, C. Chen, M. Drees, F. Paige, X. Tata, Phys. Rev. D59 (1999) 055014.

[44] D. Denegri, W. Majerotto, L. Rurua, Phys. Rev. D60 (1999) 035008.

[45] L. Rurua, doctoral thesis, CMS 1999-103/THESIS.